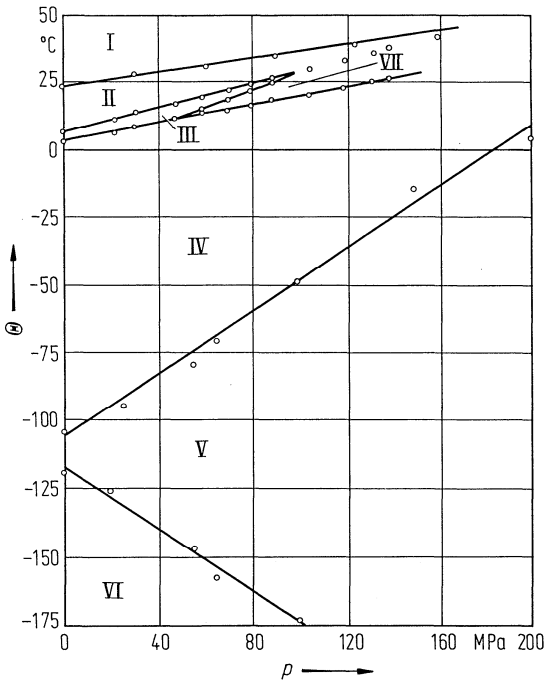

Fig. 39A-12-001. $[N(CH_3)_4]_2ZnCl_4$. Θ vs. p [80Shi].

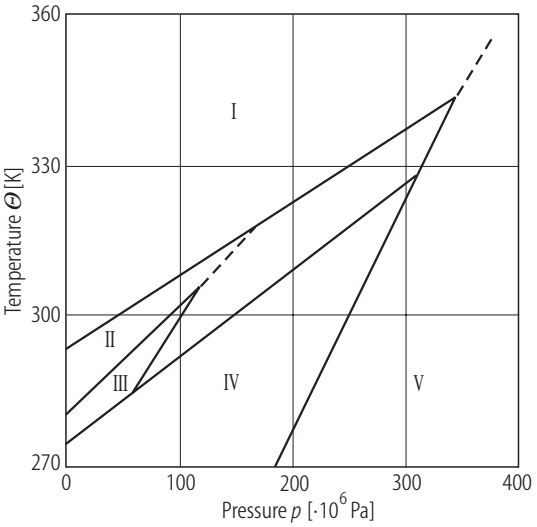

Fig. 39A-12-002. $[N(CH_3)_4]_2ZnCl_4$. Θ vs. p [90Vlo1].

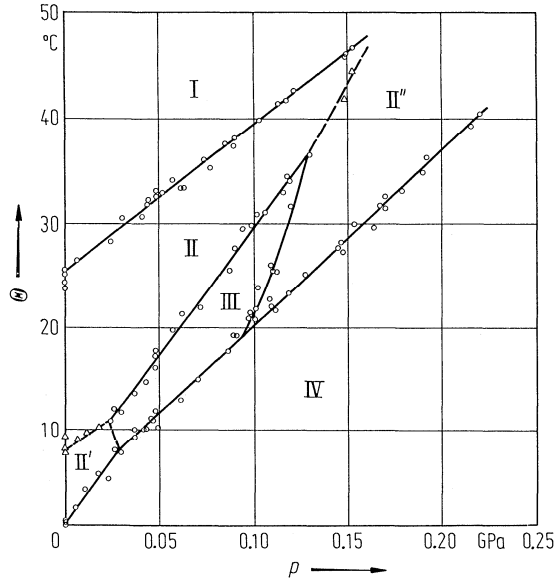

Fig. 39A-12-003. $[N(CD_3)_4]_2ZnCl_4$. Θ vs. p [82Ges2]. Triangles were plotted by slight peaks of κ_a vs. T relation in the incommensurate phase.

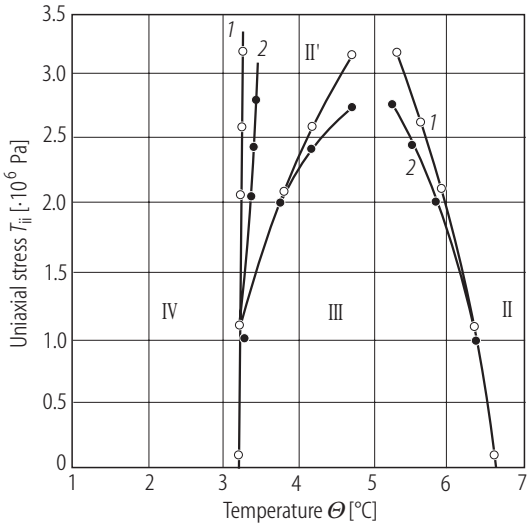

Fig. 39A-12-004. $[N(CH_3)_4]_2ZnCl_4$. Θ vs. T_{ii} [90Kal]. *1*: T_{22}, *2*: T_{33}. T_{ii}: uniaxial stress.

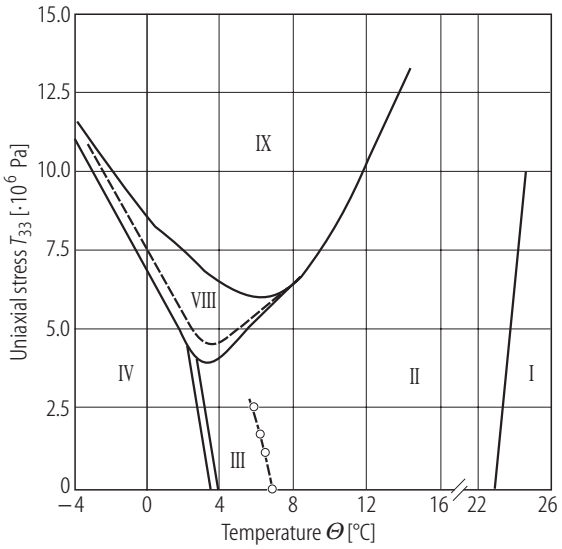

Fig. 39A-12-005. $[N(CH_3)_4]_2ZnCl_4$. Θ vs. T_{33} [92Nov]. T_{33}: uniaxial stress along the *c* axis.

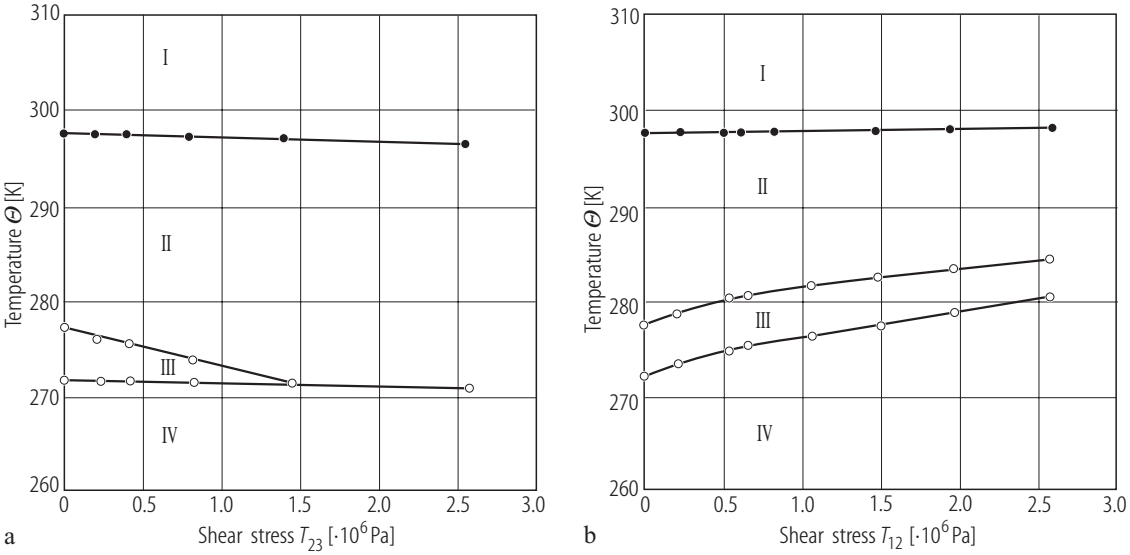

Fig. 39A-12-006. $[N(CH_3)_4]_2ZnCl_4$. Θ vs. T_{23}, T_{12} [93Sve]. T_{23}, T_{12}: shear stress.

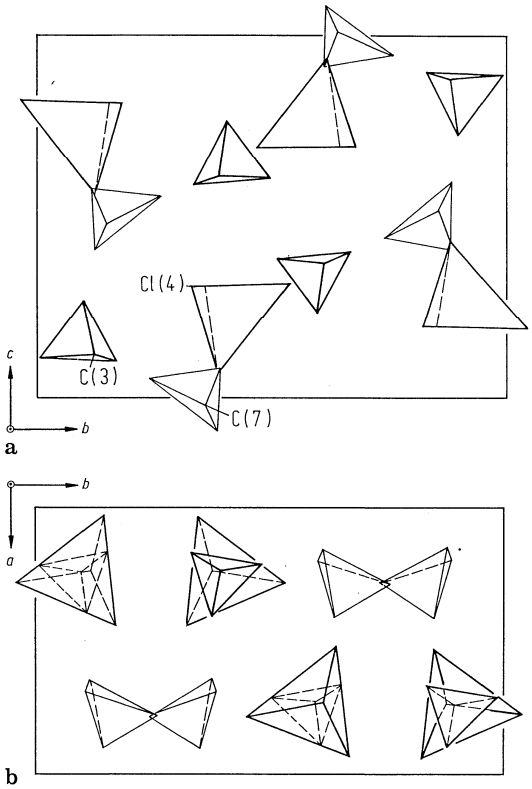

Fig. 39A-12-007. $[N(CH_3)_4]_2ZnCl_4$. Crystal structure of phase I at T = 30 °C [87Has]. Large tetrahedrons represent $ZnCl_4$ ions. Bold and thin faced small tetrahedrons represent crystallographically independent $N(CH_3)_4$ ions. Configurations related by mirrors at x = 1/4 and 3/4 are not drawn.

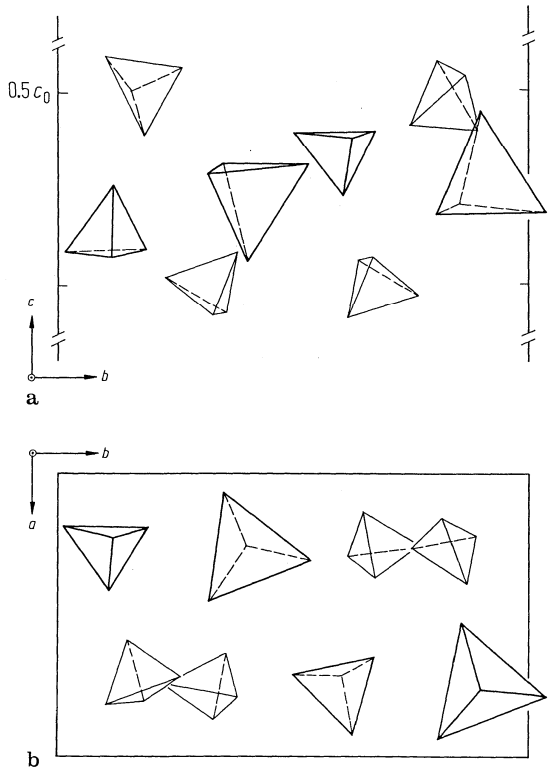

Fig. 39A-12-008. $[N(CH_3)_4]_2ZnCl_4$. Crystal structure of phase III at T = 5.5 °C [87Has]. The arrangement of ions between c = 0 and $c = 0.5c_0$, where c_0 is the basic cell dimension along the c direction. (**a**) ***a*** projection, (**b**) ***c*** projection. Large and small tetrahedrons represent $ZnCl_4$ and $N(CH_3)_4$ ions, respectively.

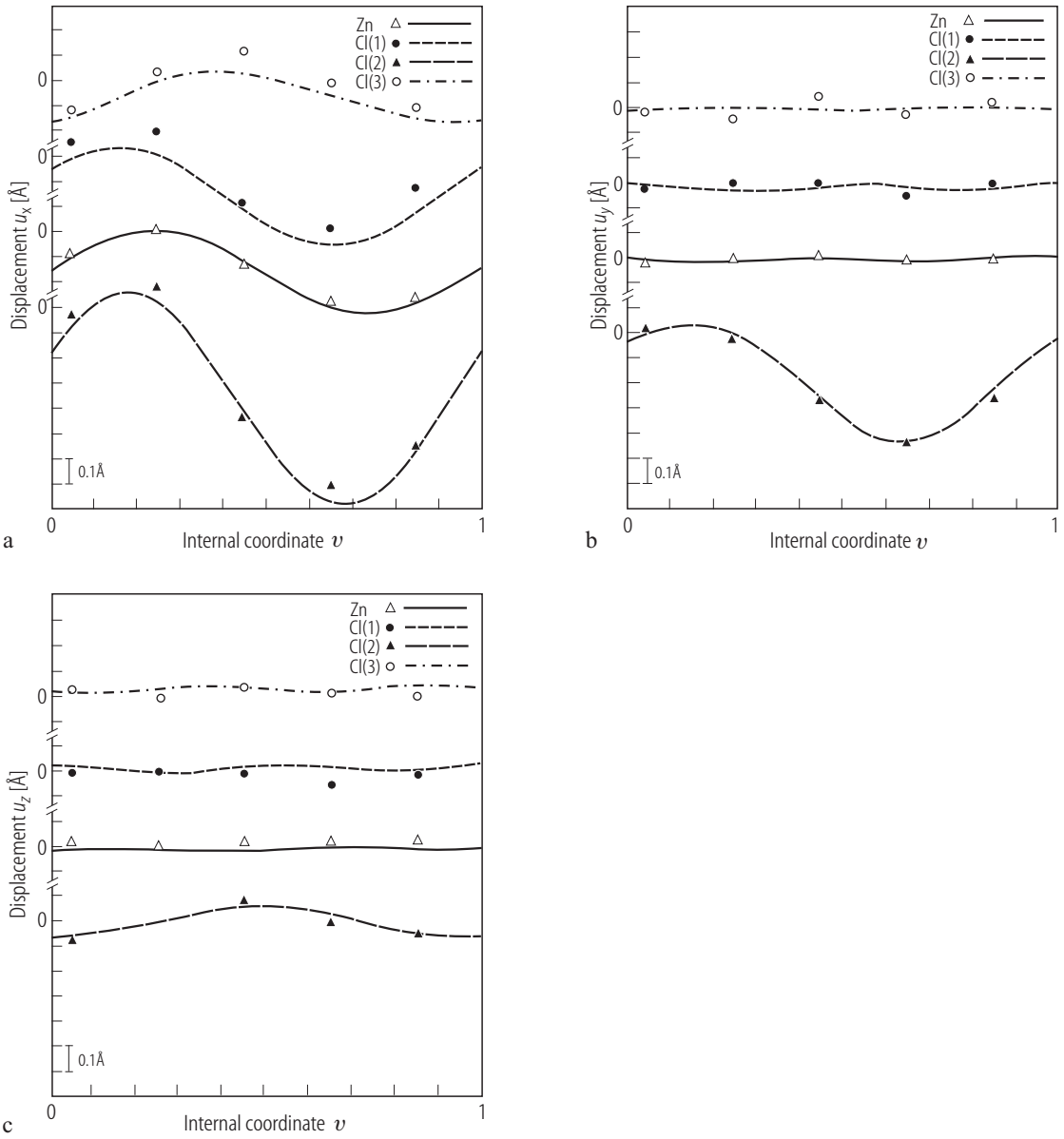

Fig. 39A-12-009. $[N(CH_3)_4]_2ZnCl_4$. Atomic displacement modulation functions along the *a*, *b* and *c* axes in phase II at T = 286.4 K (curves) and the corresponding displacements in phase III at T = 278 K (discrete points) [87Mad]. v: internal coordinate in superspace formalism. Displacements are calculated referring to the basic structure listed in Table 39A-12-004.

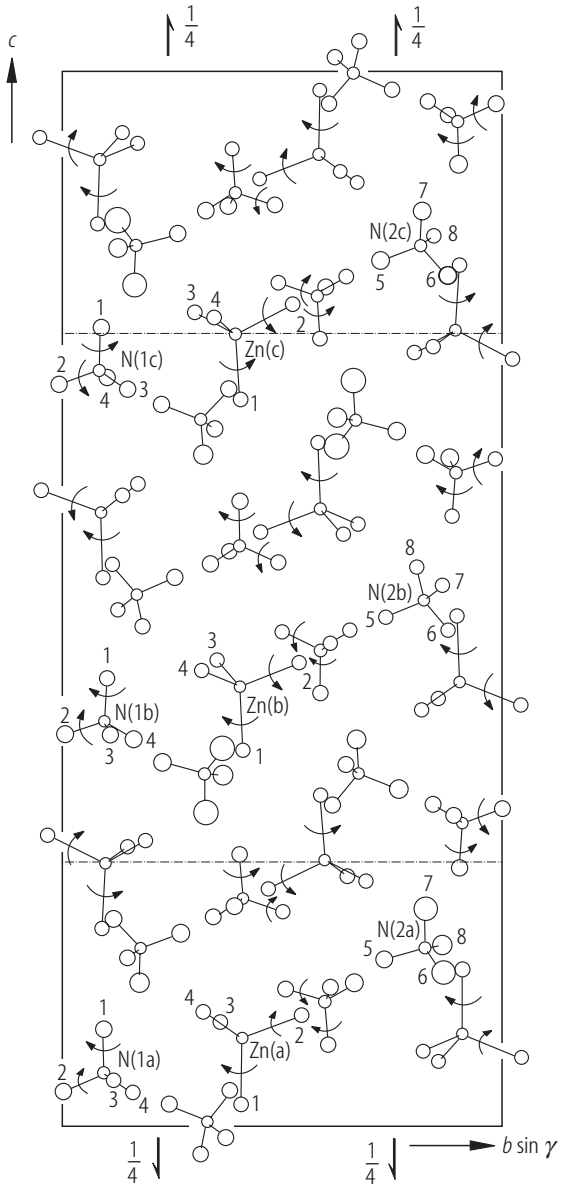

Fig. 39A-12-010. $[N(CH_3)_4]_2ZnCl_4$. Crystal structure of phase IV at T = 223 K [92Kas]. [100] projection. Circles around Zn and N atoms represent Cl and C atoms, respectively. The radius of the circle represents the mean thermal displacement estimated from the temperature parameters. The arrows indicate the direction of rotation of $ZnCl_4$ and $N(CH_3)_4$-1 about the b and c axes.

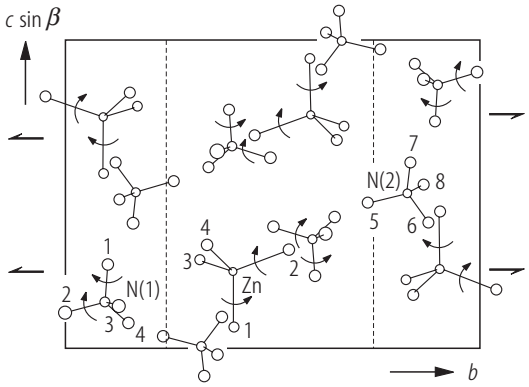

Fig. 39A-12-011. $[N(CH_3)_4]_2ZnCl_4$. Crystal structure of phase V at T = 161 K [92Kas]. [100] projection. See the caption of Fig. 39A-12-010 for the meaning of symbols.

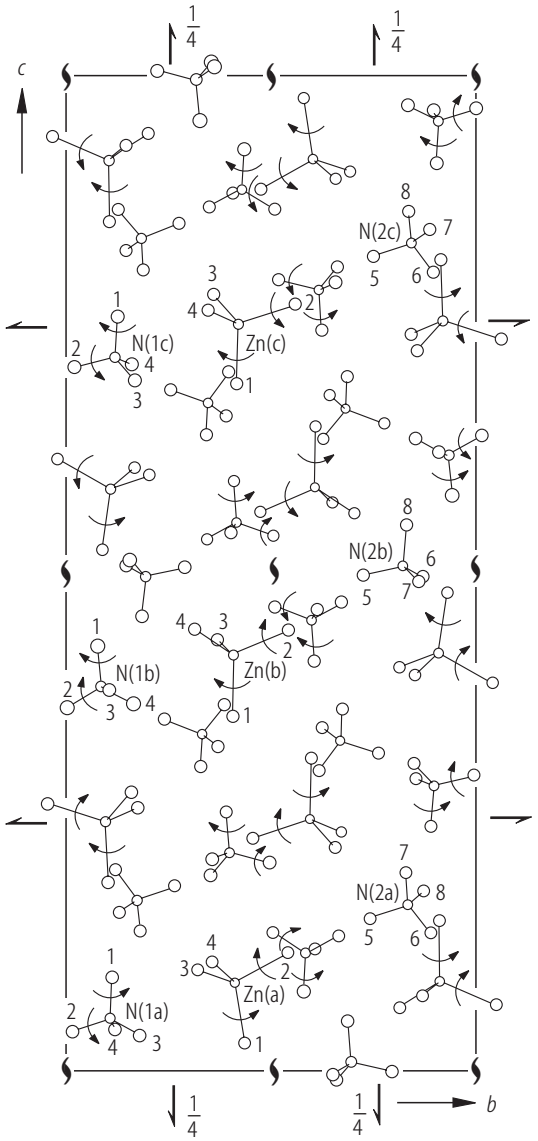

Fig. 39A-12-012. $[N(CH_3)_4]_2ZnCl_4$. Crystal structure of phase VI at T = 149 K [92Kas]. [100] projection. See the caption of Fig. 39A-12-010 for the meaning of symbols.

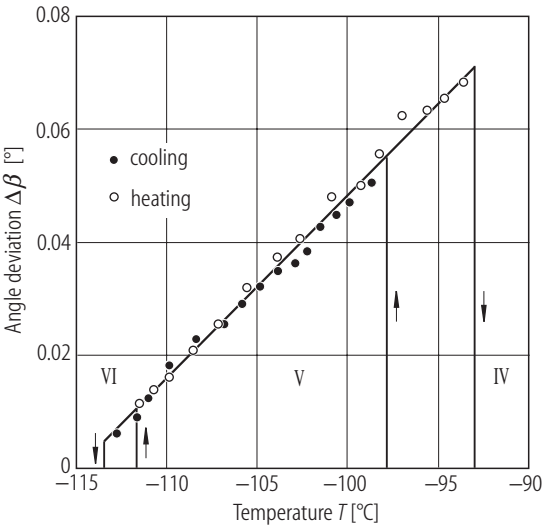

Fig. 39A-12-013. $[N(CH_3)_4]_2ZnCl_4$. $\Delta\beta$ vs. T [85Deg]. $\Delta\beta$: deviation of axial angle β from 90°.

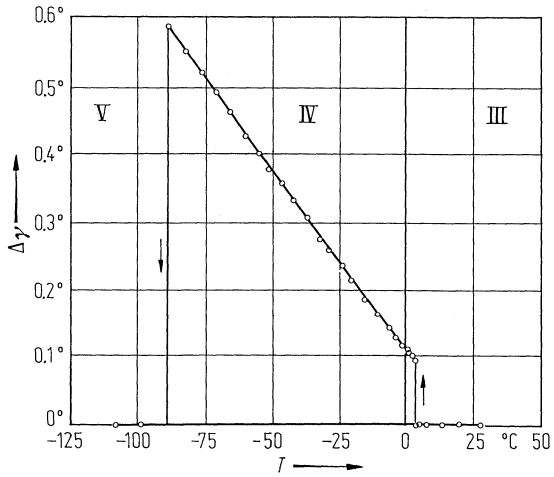

Fig. 39A-12-014. $[N(CH_3)_4]_2ZnCl_4$. $\Delta\gamma$ vs. T [85Deg]. $\Delta\gamma$: deviation of axial angle γ from 90°.

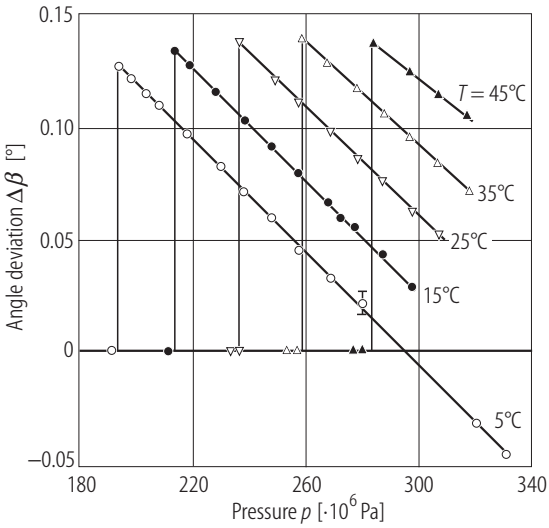

Fig. 39A-12-015. $[N(CH_3)_4]_2ZnCl_4$. $\Delta\beta$ vs. p [95Shi]. $\Delta\beta$: deviation of axial angle β from 90°. Parameter: T.

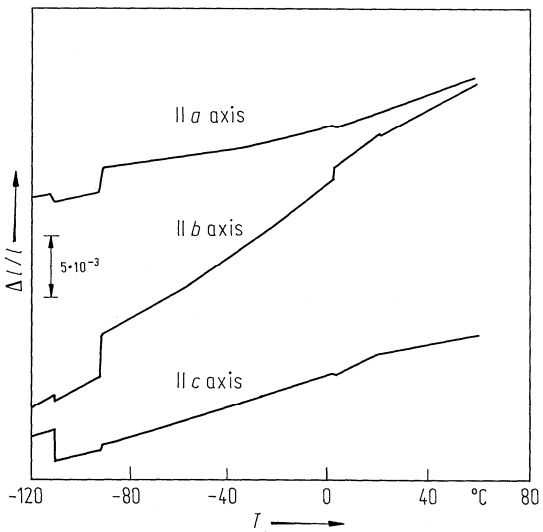

Fig. 39A-12-016. $[N(CH_3)_4]_2ZnCl_4$. $\Delta l/l$ vs. T [85Saw]. $\Delta l/l$: linear thermal expansion.

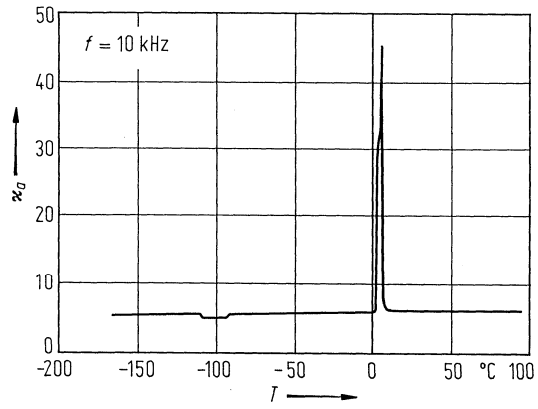

Fig. 39A-12-017. $[N(CH_3)_4]_2ZnCl_4$. κ_a vs. T [85Saw]. f = 10 kHz. On heating.

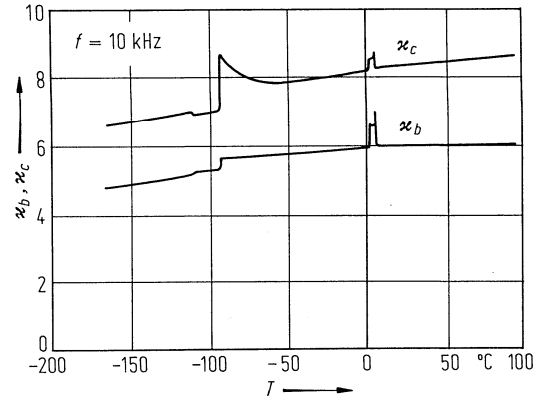

Fig. 39A-12-018. $[N(CH_3)_4]_2ZnCl_4$. κ_b, κ_c vs. T [85Saw]. f = 10 kHz. On heating.

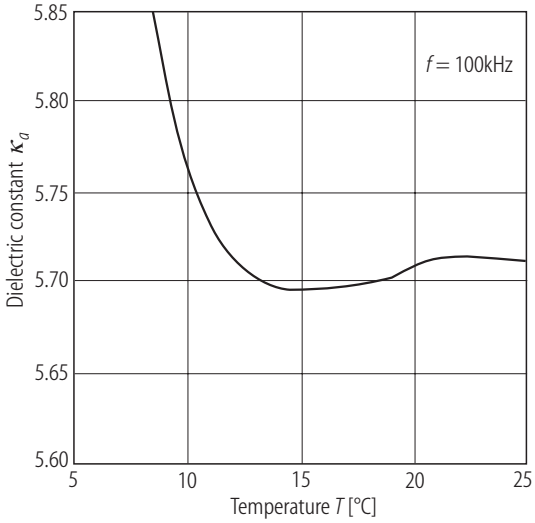

Fig. 39A-12-019. $[N(CH_3)_4]_2ZnCl_4$. κ_a vs. T [85Saw]. f = 100 kHz. On heating.

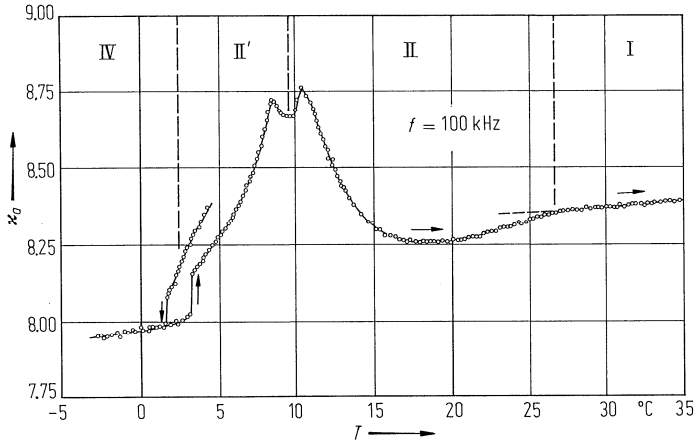

Fig. 39A-12-020. $[N(CD_3)_4]_2ZnCl_4$. κ_a vs. T [82Ges1]. f = 100 kHz. The peak around 10 °C did not split in some specimens. See subsection 14a of the survey table.

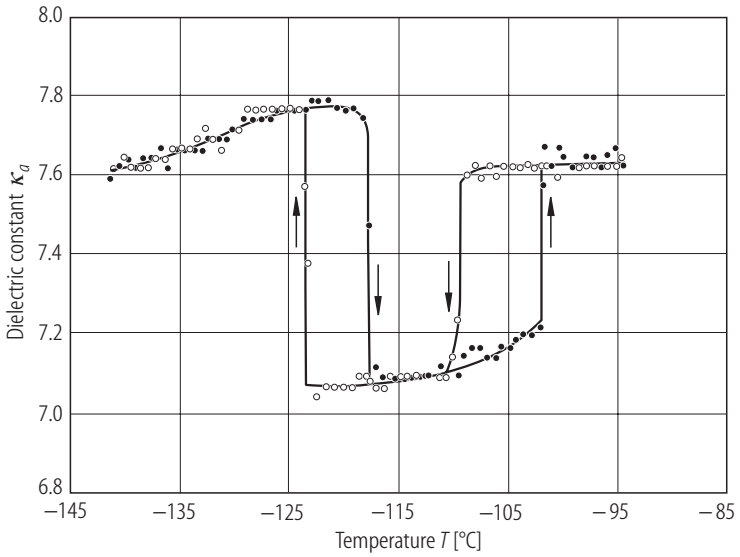

Fig. 39A-12-021. $[N(CD_3)_4]_2ZnCl_4$. κ_a vs. T [82Ges1]. f = 100 kHz. Open circles: on cooling, closed circles: on heating.

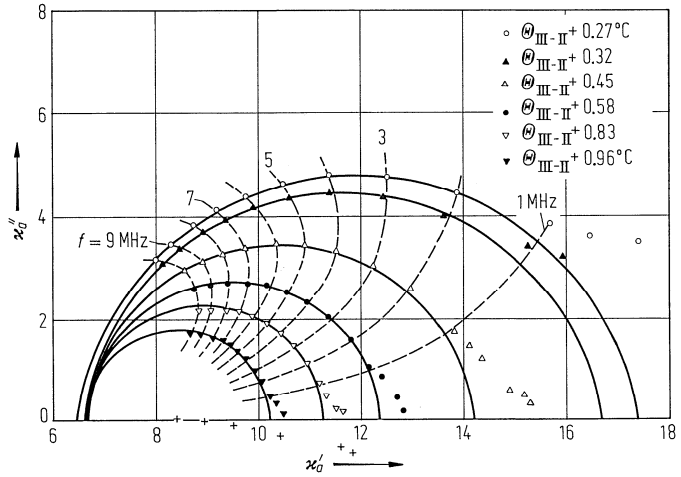

Fig. 39A-12-022. $[N(CH_3)_4]_2ZnCl_4$. Cole-Cole plot of the complex dielectric constant above Θ_{III-II} [83Hor]. Plus sign: centers of the circular arcs.

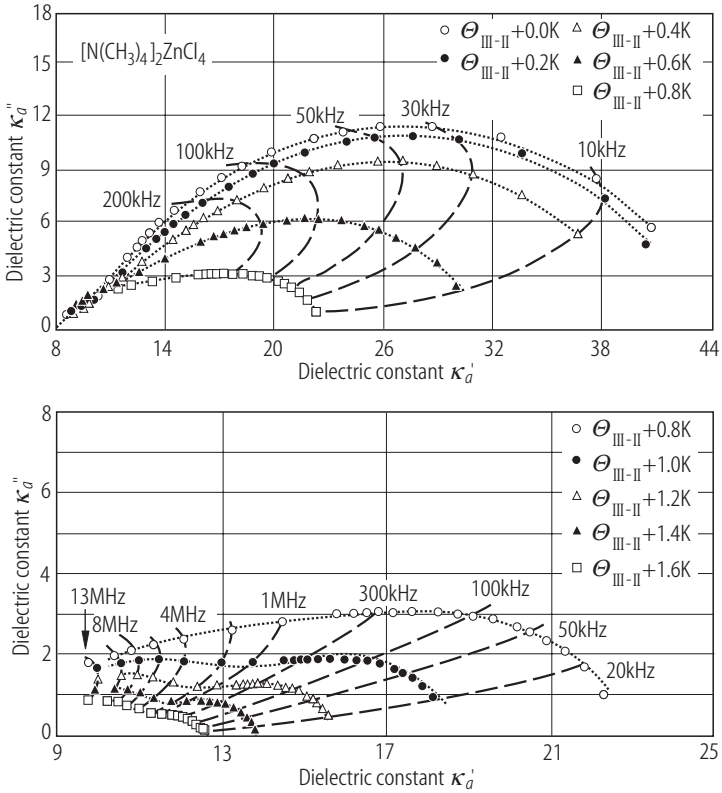

Fig. 39A-12-023. $[N(CH_3)_4]_2ZnCl_4$. Cole-Cole plot of the complex dielectric constant above Θ_{III-II} [90LeV].

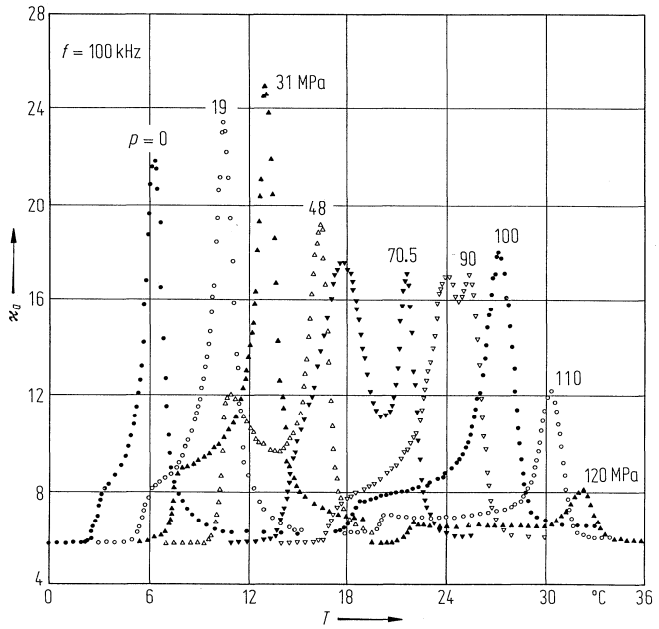

Fig. 39A-12-024. $[N(CH_3)_4]_2ZnCl_4$. κ_a vs. T [80Shi]. Parameter: p. f = 100 kHz. On cooling.

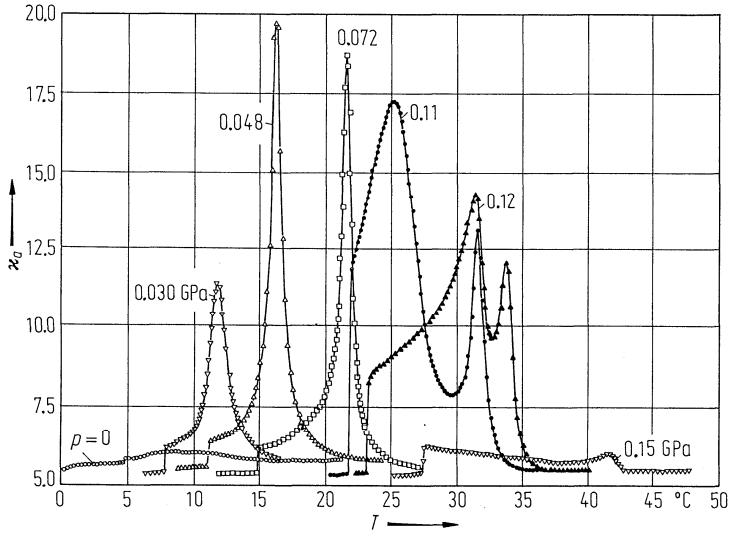

Fig. 39A-12-025. $[N(CD_3)_4]_2ZnCl_4$. κ_a vs. T [82Ges2]. Parameter: p. f = 100 kHz.

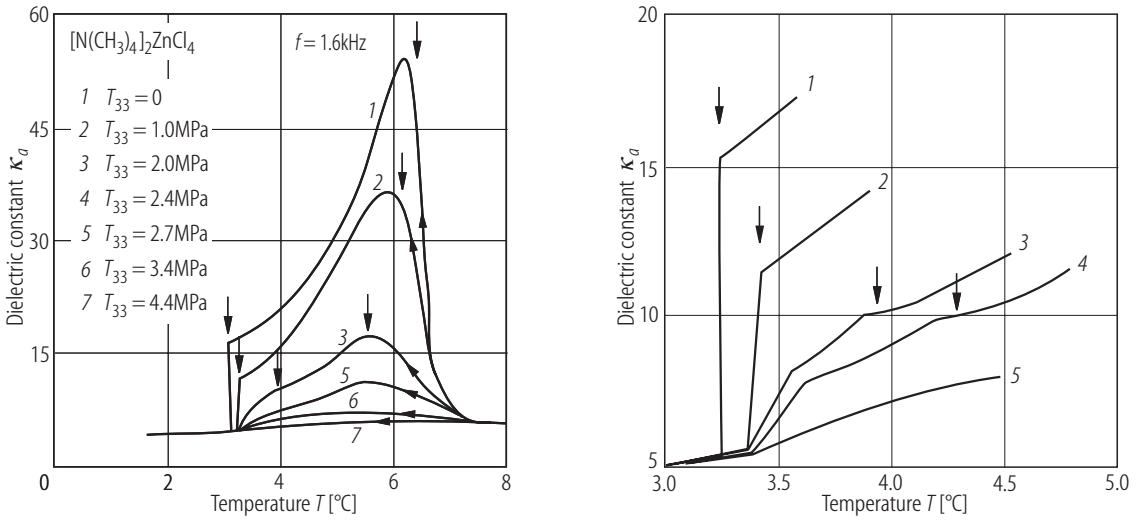

Fig. 39A-12-026. $[N(CH_3)_4]_2ZnCl_4$. κ_a vs. T [90Kal]. Parameter: T_{33}. T_{33}: uniaxial stress along the c axis. Arrows indicate the high- and low-temperature boundaries of ferroelectric phase.

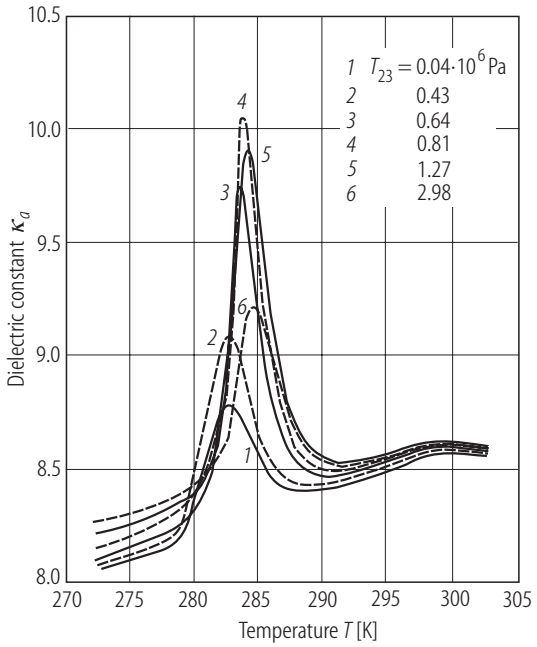

Fig. 39A-12-027. $[N(CD_3)_4]_2ZnCl_4$. κ_a vs. T [91Kro]. Parameter: T_{23}. T_{23}: shear stress.

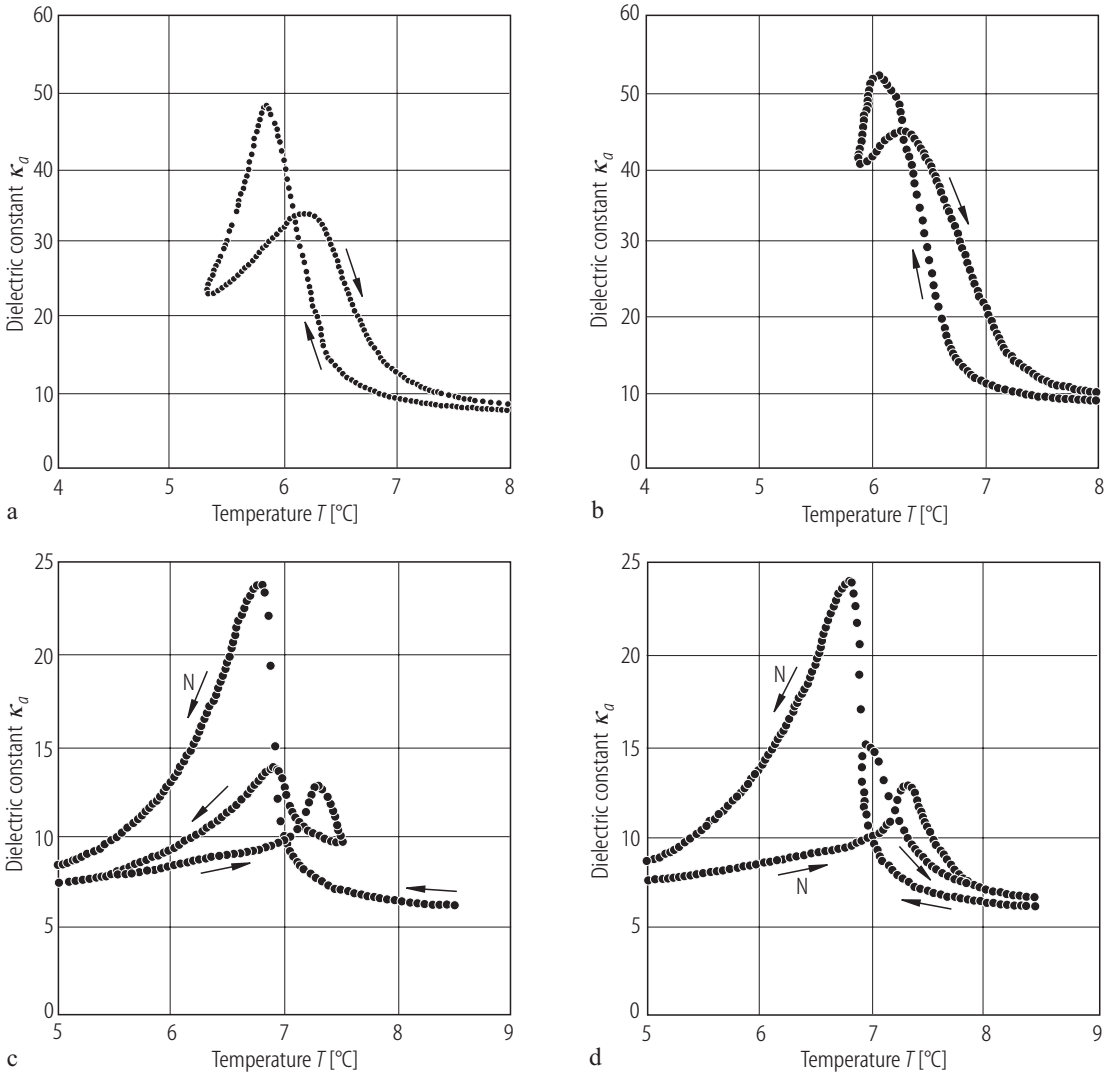

Fig. 39A-12-028. $[N(CH_3)_4]_2ZnCl_4$. κ_a vs. T [90Fol]. Cooling runs are inverted to heating runs in (**a**), (**b**), (**d**) and vice versa in (**c**). The normal behavior, denoted as N, is shown in (**c**) and (**d**) for comparison.

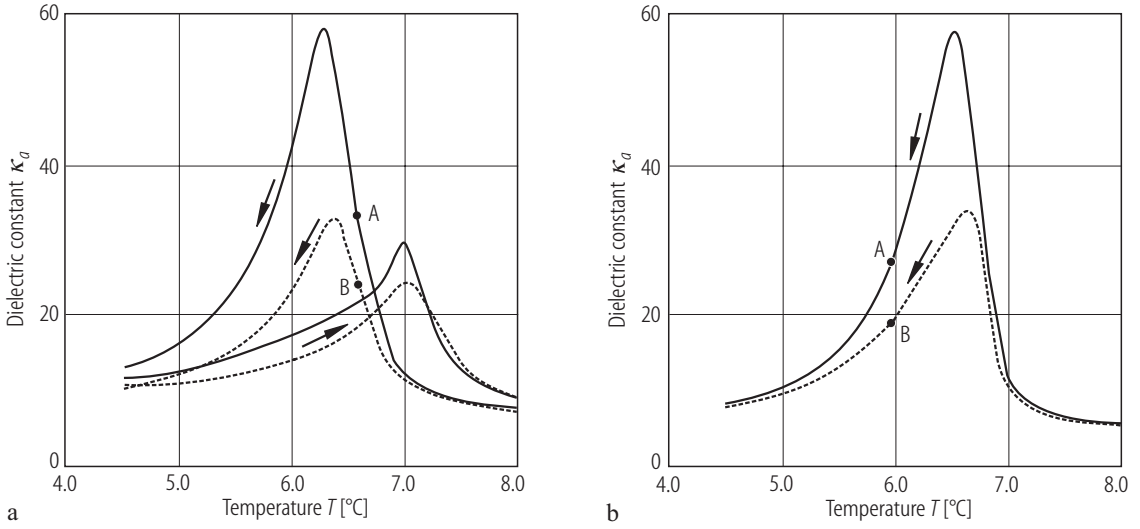

Fig. 39A-12-029. $[N(CH_3)_4]_2ZnCl_4$. κ_a vs. T after annealed at point A for (**a**) 7 hours and (**b**) 5 hours [90Fol]. B: annealing point after relaxation. The solid line represents the normal behavior.

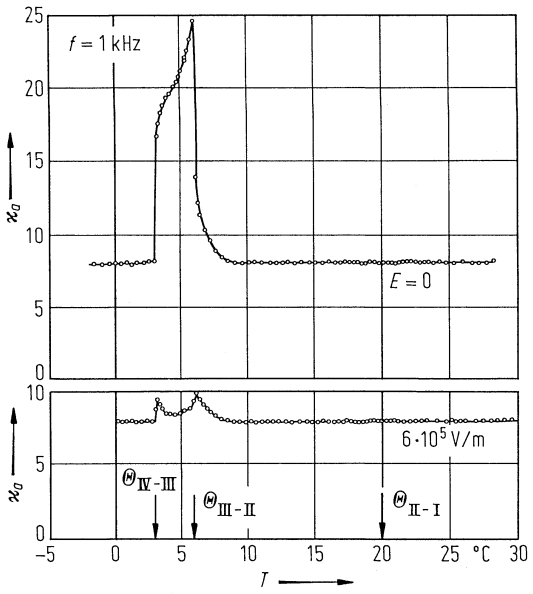

Fig. 39A-12-030. $[N(CH_3)_4]_2ZnCl_4$. κ_a vs. T [85Sai]. Parameter: E_{bias}. f = 1 kHz. On heating.

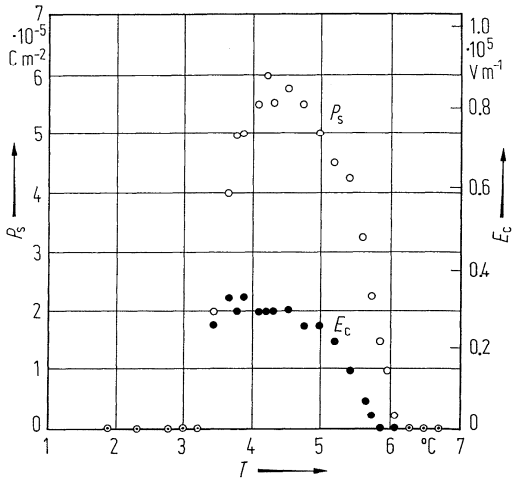

Fig. 39A-12-031. $[N(CH_3)_4]_2ZnCl_4$. P_s, E_c vs. T [78Saw1]. On heating.

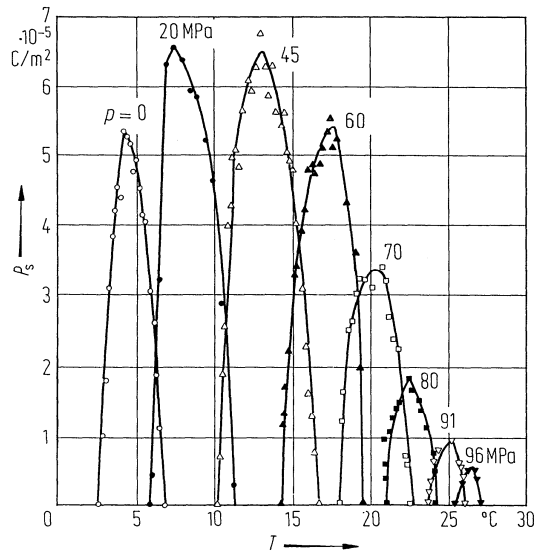

Fig. 39A-12-032. $[N(CH_3)_4]_2ZnCl_4$. P_s vs. T [80Shi]. Parameter: p. On cooling.

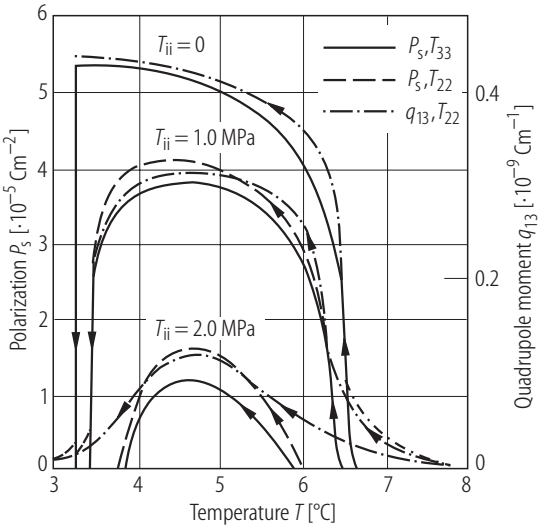

Fig. 39A-12-033. $[N(CH_3)_4]_2ZnCl_4$. P_s, q_{13} vs. T [90Kal]. Parameter: T_{22}, T_{33}. T_{ii}: uniaxial stress. q_{13}: macroscopic quadrupole moment.

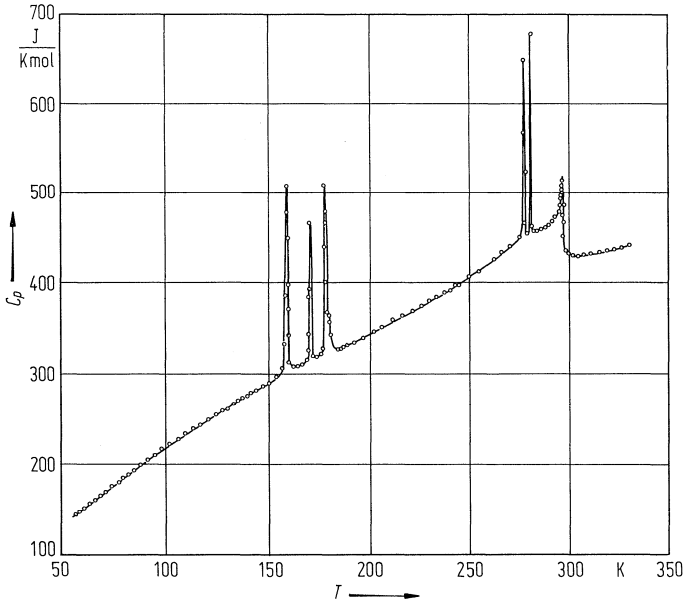

Fig. 39A-12-034. $[N(CH_3)_4]_2ZnCl_4$. C_p vs. T [81Rui]. C_p: molar heat capacity at constant pressure.

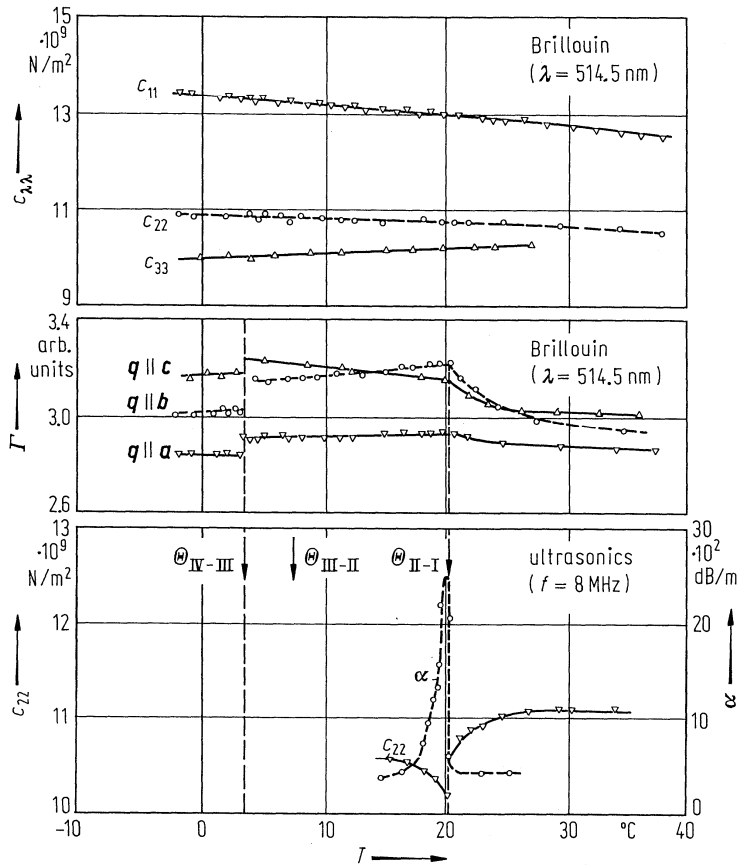

Fig. 39A-12-035. $[N(CH_3)_4]_2ZnCl_4$. $c_{\lambda\lambda}$, Γ, α vs. T [84Ber]. Γ: attenuation of longitudinal phonon. α: sound attenuation coefficient of c_{22} mode.

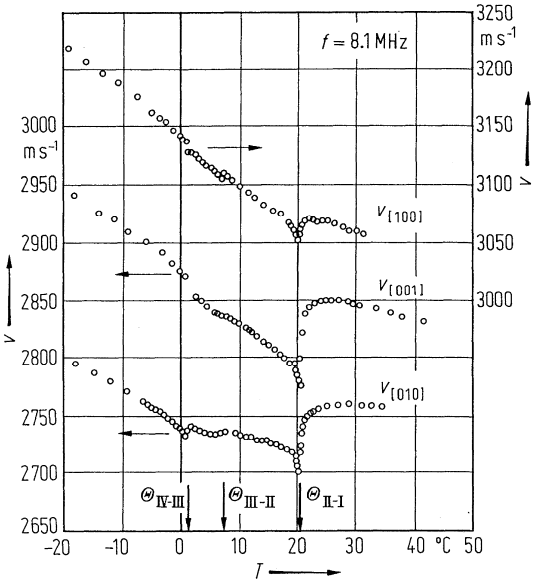

Fig. 39A-12-036. $[N(CH_3)_4]_2ZnCl_4$. v vs. T [79Hos]. v: sound velocity of longitudinal mode at 8.1 MHz. On cooling.

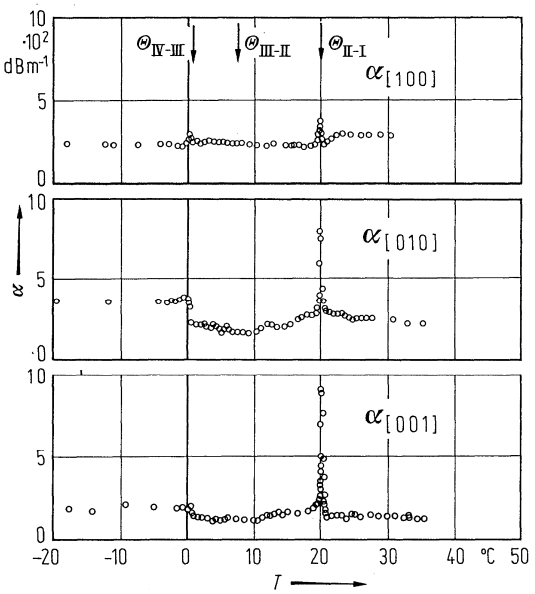

Fig. 39A-12-037. $[N(CH_3)_4]_2ZnCl_4$. α vs. T [79Hos]. α: sound attenuation coefficient of longitudinal mode at 8.1 MHz.

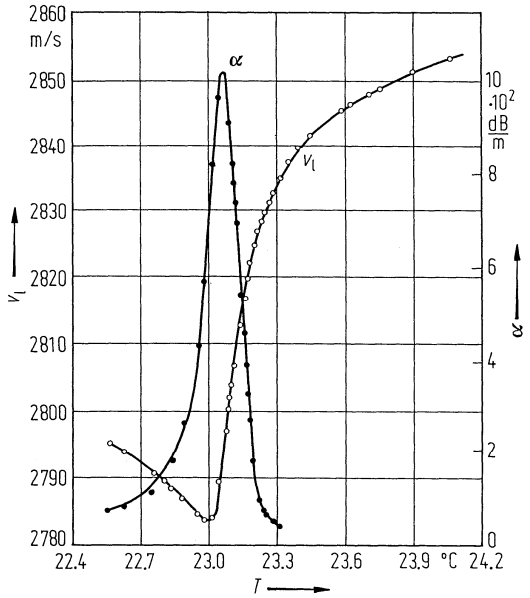

Fig. 39A-12-038. $[N(CH_3)_4]_2ZnCl_4$. υ_l, α vs. T [86Ber]. υ_l: sound velocity, $\upsilon_l = (c_{33}/\rho)^{1/2}$. α: sound attenuation coefficient of c_{33} mode. $f = 10$ MHz.

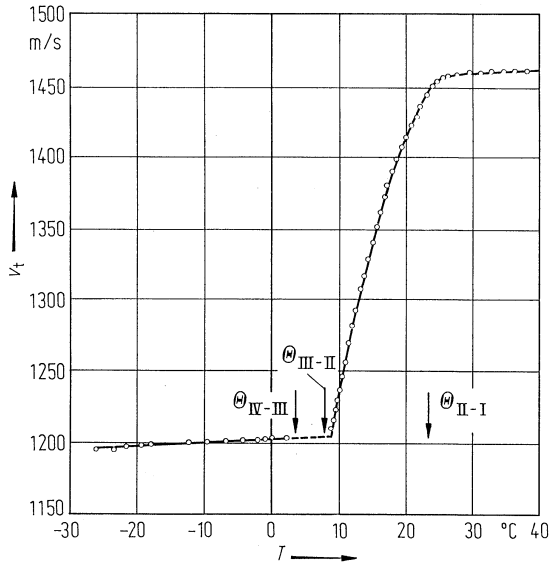

Fig. 39A-12-039. $[N(CH_3)_4]_2ZnCl_4$. v_t vs. T [86Ber]. v_t: sound velocity, $v_t = (c_{44}/\rho)^{1/2}$. $f = 10$ MHz.

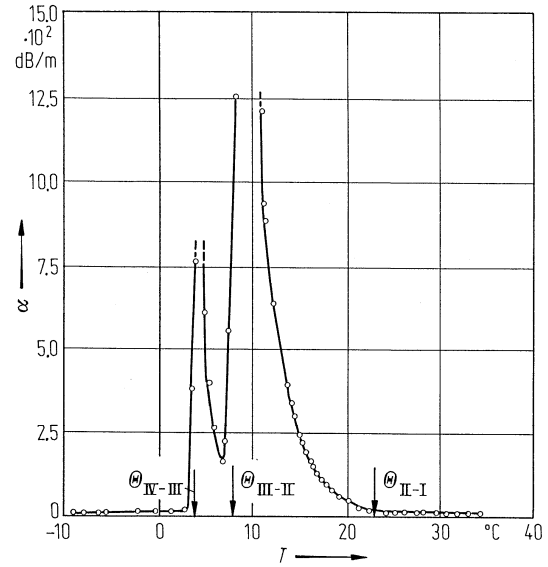

Fig. 39A-12-040. $[N(CH_3)_4]_2ZnCl_4$. α vs. T [86Ber]. α: sound attenuation coefficient of c_{44} shear mode. $f = 10$ MHz.

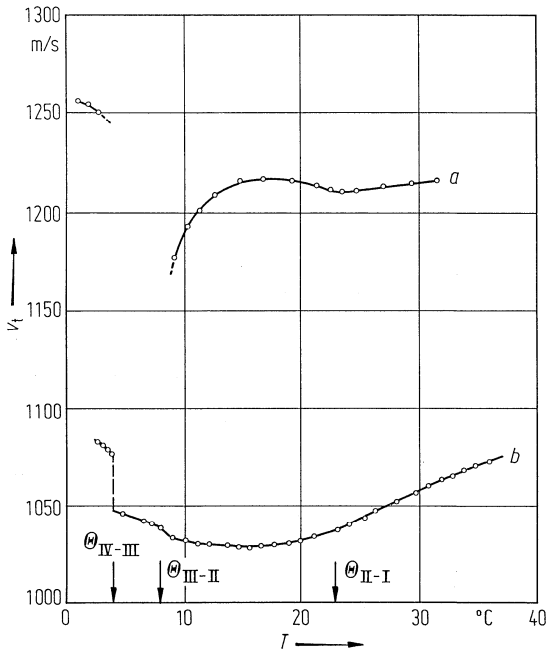

Fig. 39A-12-041. $[N(CH_3)_4]_2ZnCl_4$. υ_t vs. T [86Ber]. υ_t: sound velocity. Curve *a*: $\upsilon_t = (c_{66}/\rho)^{1/2}$, *b*: $\upsilon_t = (c_{55}/\rho)^{1/2}$. $f = 10$ MHz.

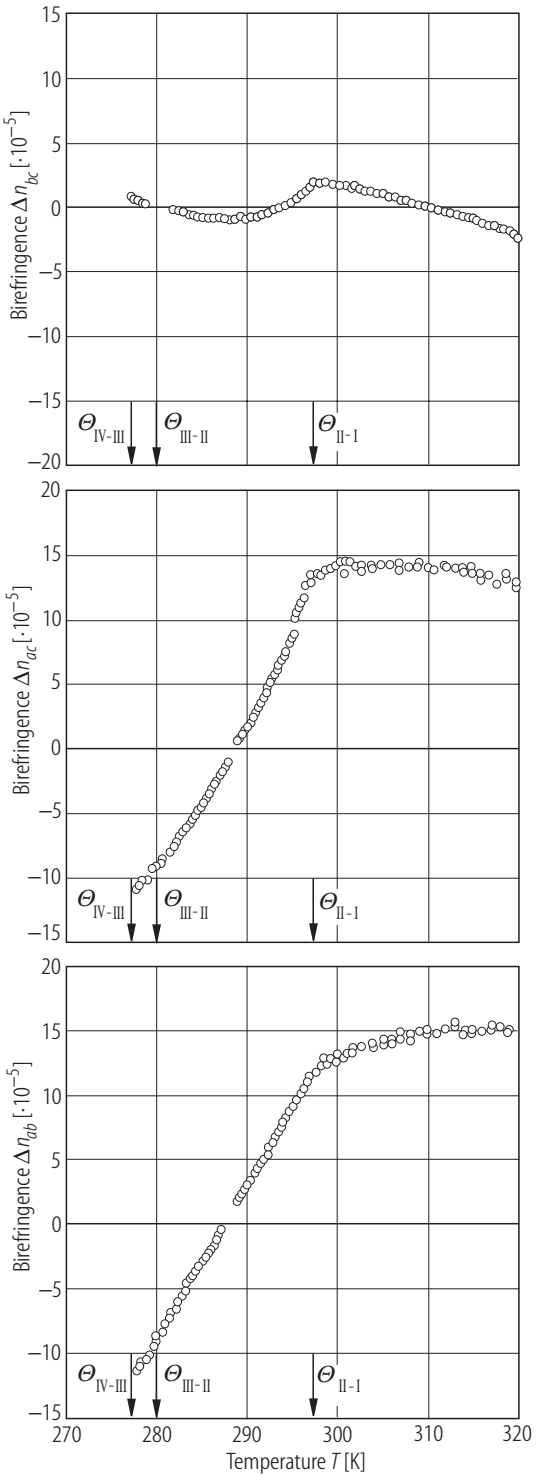

Fig. 39A-12-042. $[N(CH_3)_4]_2ZnCl_4$. Δn vs. T [93Kob]. $\lambda = 632.8$ nm.

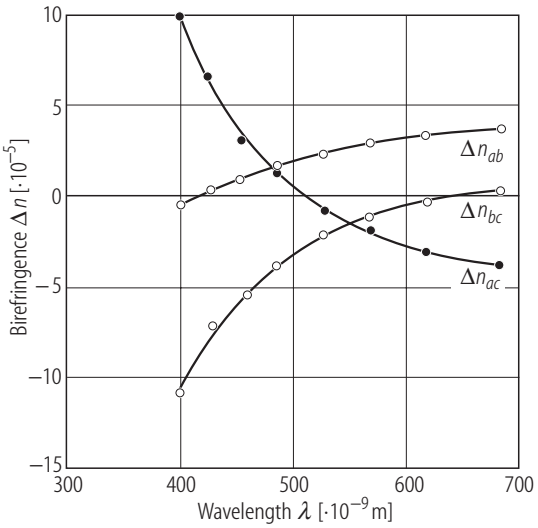

Fig. 39A-12-043. $[N(CH_3)_4]_2ZnCl_4$. Δn vs. λ at 292 K [87Vlo]. Δn_{ab}, Δn_{bc}, Δn_{ac}: birefringence in the *ab*, *bc*, *ac* plane, respectively.

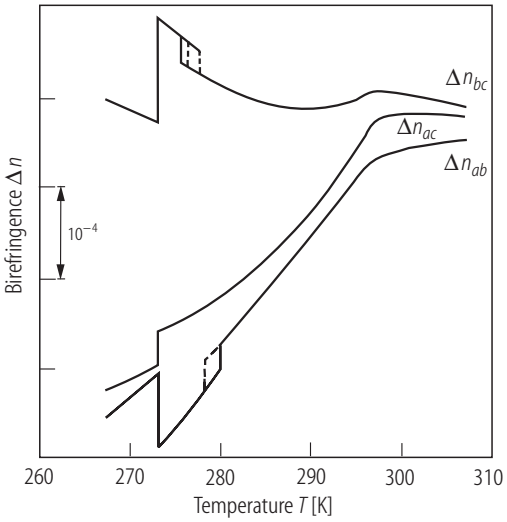

Fig. 39A-12-044. $[N(CD_3)_4]_2ZnCl_4$. Δn vs. T [91Kro]. $\Delta n_{bc} = n_b - n_c$, $\Delta n_{ac} = n_a - n_c$, $\Delta n_{ab} = n_a - n_b$. $\lambda = 632.8$ nm.

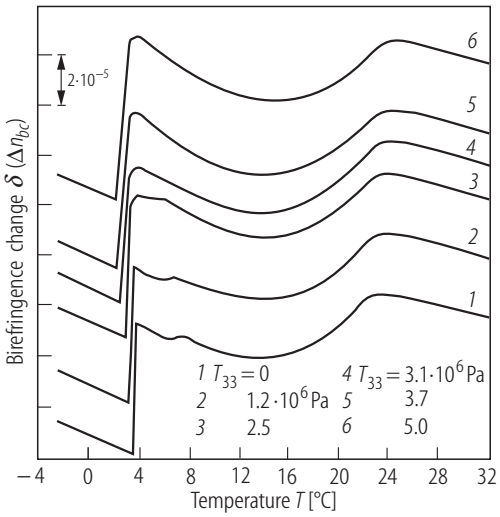

Fig. 39A-12-045. $[N(CH_3)_4]_2ZnCl_4$. $\delta(\Delta n_{bc})$ vs. T [92Nov]. $\delta(\Delta n_{bc})$: change in birefringence in the bc plane. Parameter: T_{33}. T_{33}: uniaxial stress along the c axis. $\lambda = 632.8$ nm.

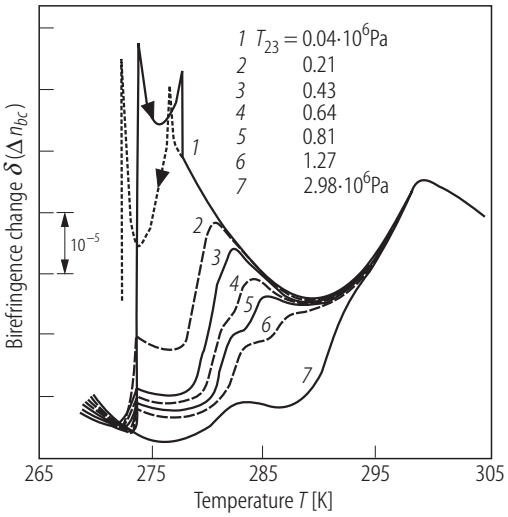

Fig. 39A-12-046. $[N(CD_3)_4]_2ZnCl_4$. $\delta(\Delta n_{bc})$ vs. T [91Kro]. $\delta(\Delta n_{bc})$: change in birefringence in the bc plane. Parameter: T_{23}. T_{23}: shear stress. $\lambda = 632.8$ nm.

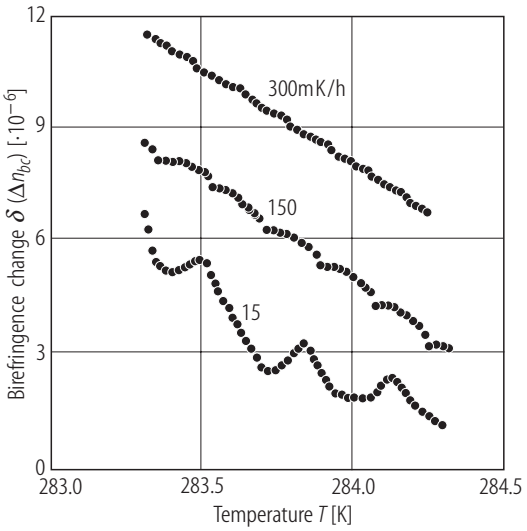

Fig. 39A-12-047. $[N(CH_3)_4]_2ZnCl_4$. $\delta(\Delta n_{bc})$ vs. T [91Vlo1]. $\delta(\Delta n_{bc})$: change in birefringence in the bc plane. Parameter: heating rate. $\lambda = 632.8$ nm.

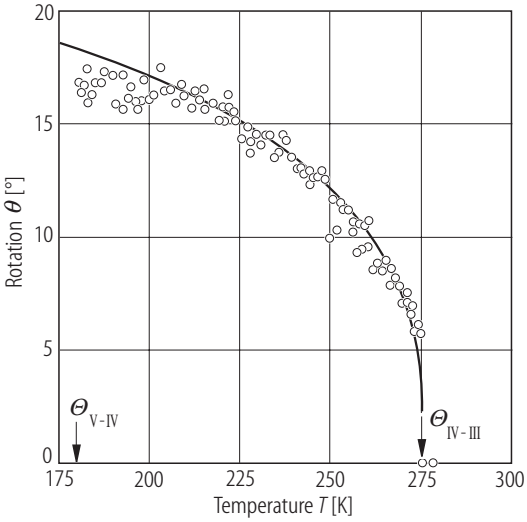

Fig. 39A-12-048. $[N(CH_3)_4]_2ZnCl_4$. θ vs. T in phase IV [88Mee]. θ: rotation angle of the indicatrix for white light.

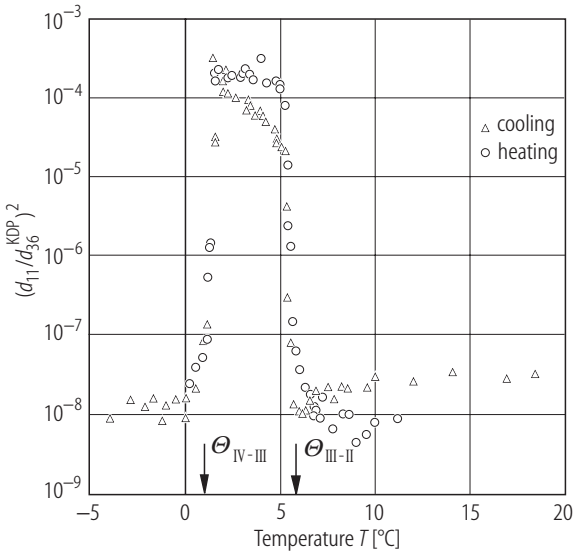

Fig. 39A-12-049. $[N(CH_3)_4]_2ZnCl_4$. $(d_{11}/d_{36}^{KDP})^2$ vs. T [92Ues]. $d_{i\lambda}$: susceptibility for second harmonic generation. Wave length of the fundamental wave is 1.06 μm.

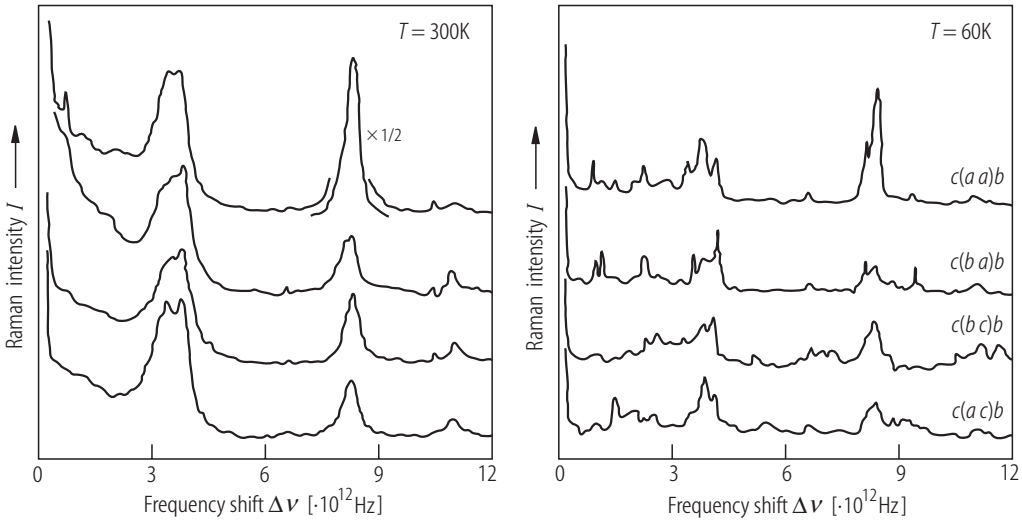

Fig. 39A-12-050. $[N(CH_3)_4]_2ZnCl_4$. I vs. $\Delta\nu$ in phase I (300 K) and in phase VI (60 K) [88Mee]. I: Raman scattering intensity. Parameter: scattering geometry.

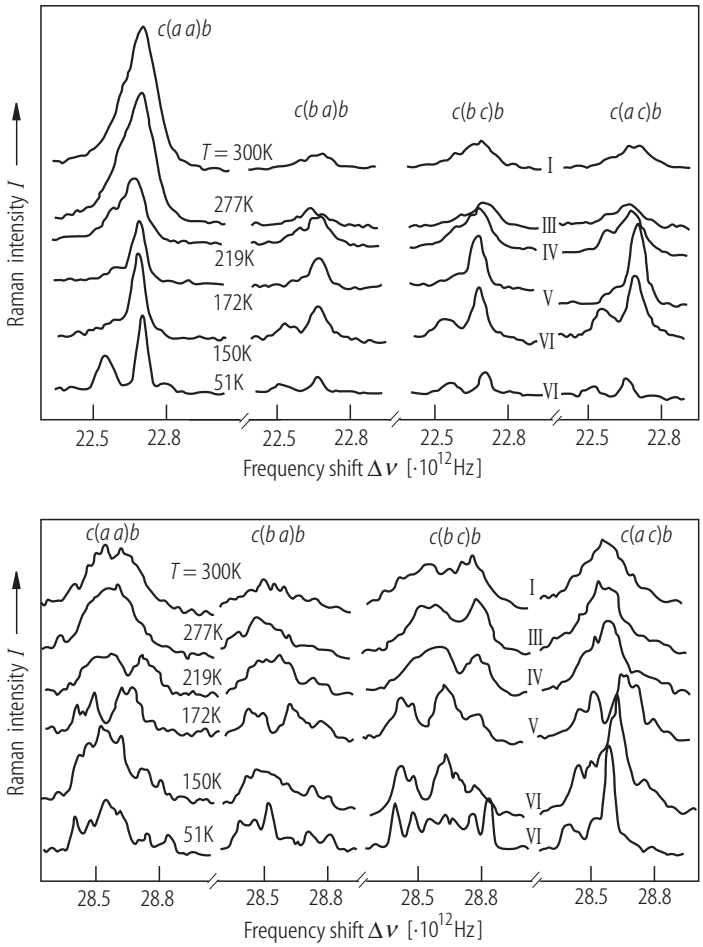

Fig. 39A-12-051. $[N(CH_3)_4]_2ZnCl_4$. I vs. $\Delta\nu$ [88Mee]. I: Raman scattering intensity. Parameter: T. In phase IV, instead of the polarization (*aa*), (*bb*) should be read.

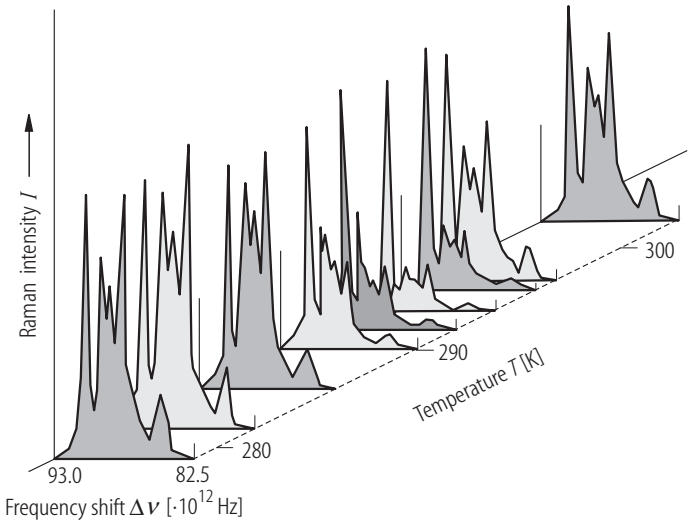

Fig. 39A-12-052. $[N(CH_3)_4]_2ZnCl_4$. Temperature dependence of Raman spectra [86Pal]. I: Raman scattering intensity. Polarization geometry: $c(bb)a$.

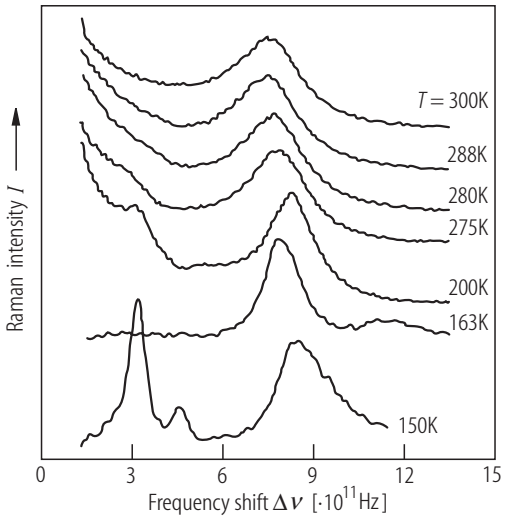

Fig. 39A-12-053. $[N(CH_3)_4]_2ZnCl_4$. I vs. $\Delta\nu$ [90Che]. I: Raman scattering intensity in (cc) geometry. Parameter: T. The Rayleigh wing has been subtracted.

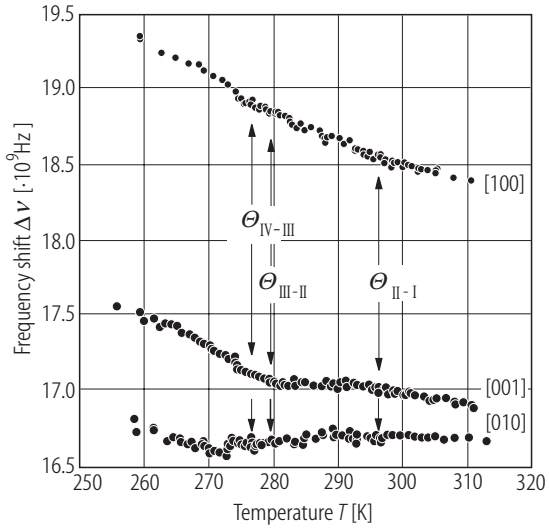

Fig. 39A-12-054. $[N(CH_3)_4]_2ZnCl_4$. $\Delta\nu$ vs. T [90Yos]. $\Delta\nu$: Brillouin frequency shift of the longitudinal modes. $\lambda = 514.5$ nm. Back scattering.

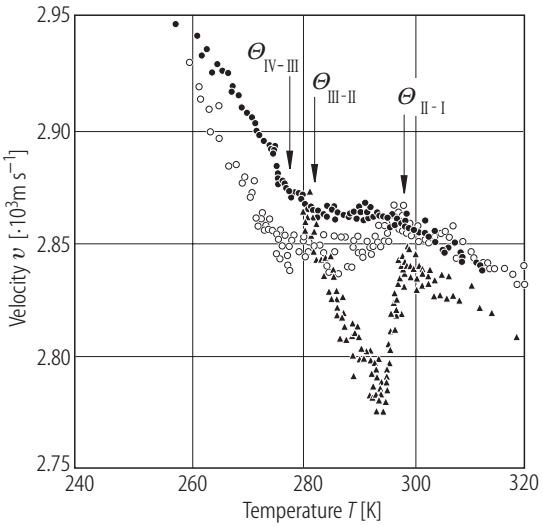

Fig. 39A-12-055. $[N(CH_3)_4]_2ZnCl_4$. v vs. T [90Yos]. v: [001] LA-phonon velocity measured by Brillouin scattering. Full circle: back scattering ($\nu \approx 17$ GHz), open circle: right-angle scattering ($\nu \approx 12$ GHz), full triangle: forward scattering ($\nu \approx 1.45$ GHz). $\lambda = 514.5$ nm.

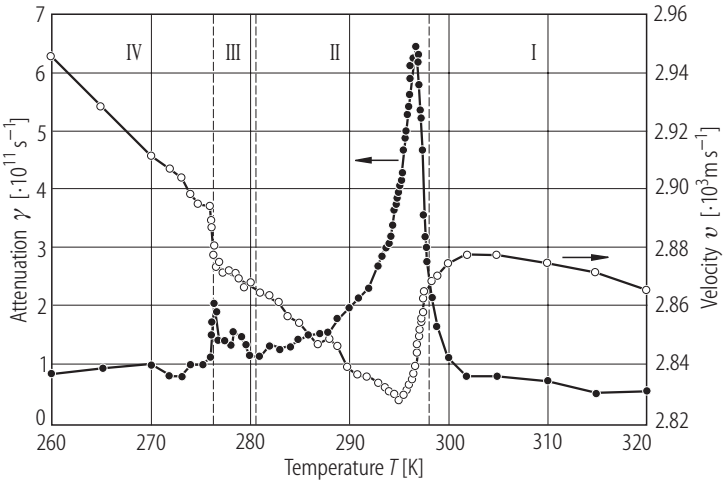

Fig. 39A-12-056. $[N(CH_3)_4]_2ZnCl_4$. γ, v vs. T [92Sil]. γ, v: acoustic attenuation rate and velocity of [001] LA-phonon with wave length $\lambda = 3.269$ μm measured by impulsive stimulated scattering.

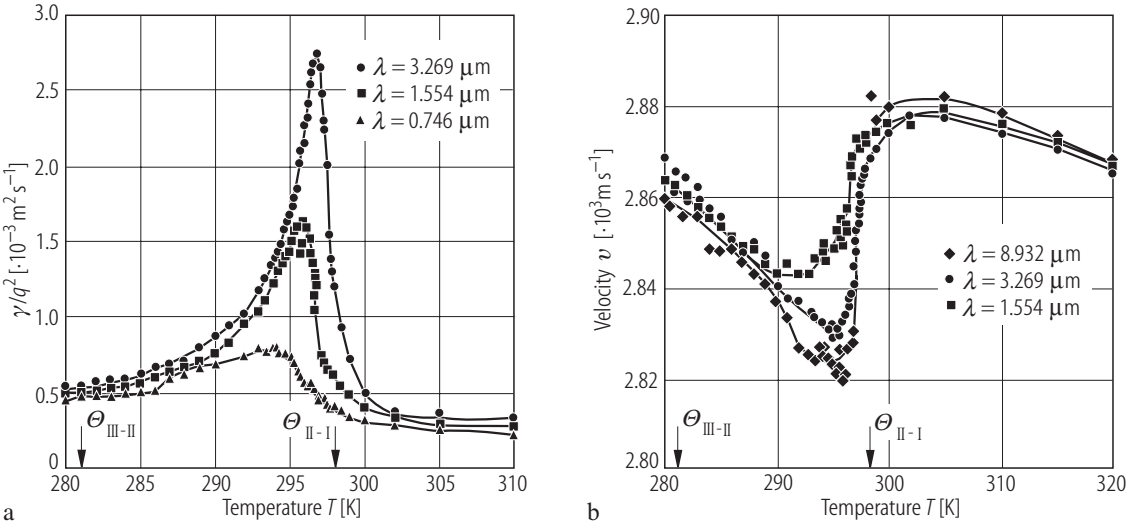

Fig. 39A-12-057. $[N(CH_3)_4]_2ZnCl_4$. (**a**) γ/q^2 vs. T, (**b**) v vs. T [92Sil]. γ, v: acoustic attenuation rate and velocity of [001] LA-phonon measured by impulsive stimulated scattering. q: wave number. Parameter: wave length.

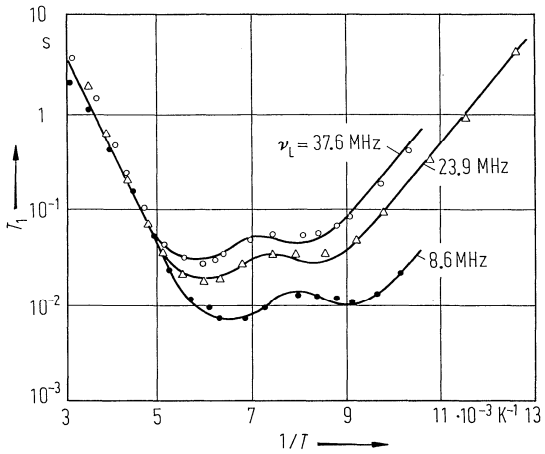

Fig. 39A-12-058. $[N(CH_3)_4]_2ZnCl_4$. T_1 vs. $1/T$ [81Nie]. T_1: ^{1}H spin-lattice relaxation time. Powder specimen.

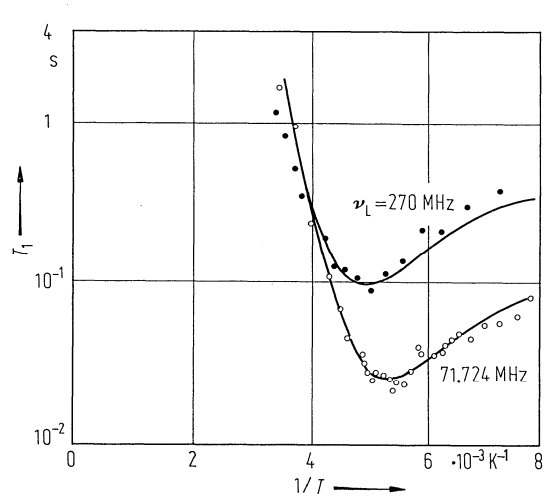

Fig. 39A-12-059. $[N(CH_3)_4]_2ZnCl_4$. T_1 vs. $1/T$ [86Dol]. T_1: ^{1}H spin-lattice relaxation time.

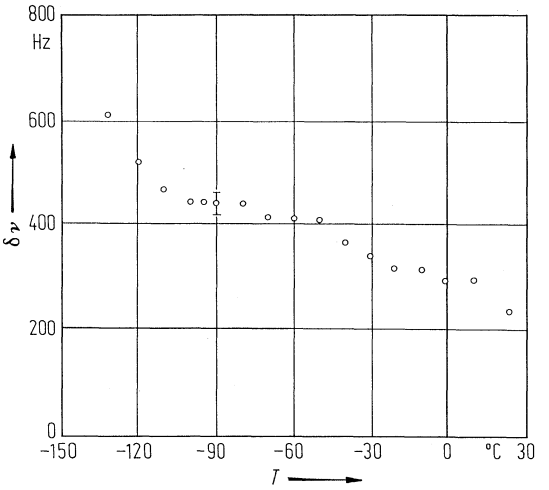

Fig. 39A-12-060. $[N(CH_3)_4]_2ZnCl_4$. $\delta\nu$ vs. T [86Dol]. $\delta\nu$: ^{13}C NMR linewidth. ν_L = 67.8 MHz.

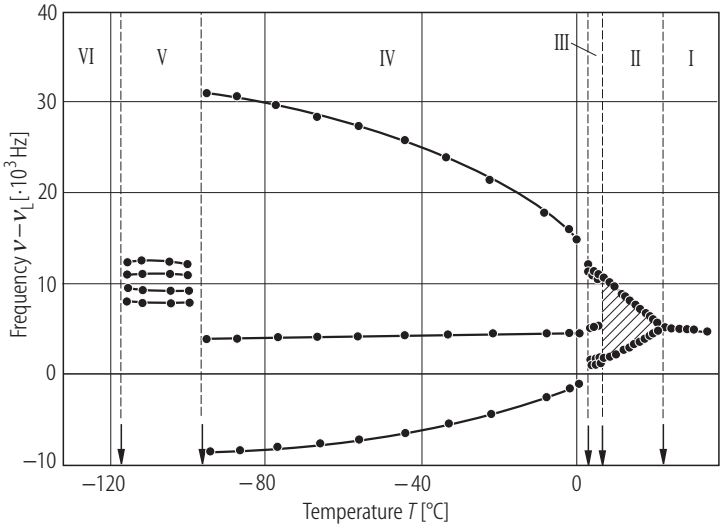

Fig. 39A-12-061. $[N(CH_3)_4]_2ZnCl_4$. $\nu - \nu_L$ vs. T [88Dol]. ν: NMR resonance frequency of ^{14}N. ν_L = 19.520 MHz. Hatched region denotes incommensurate continuous spectra. $\boldsymbol{H} \parallel \boldsymbol{b}$.

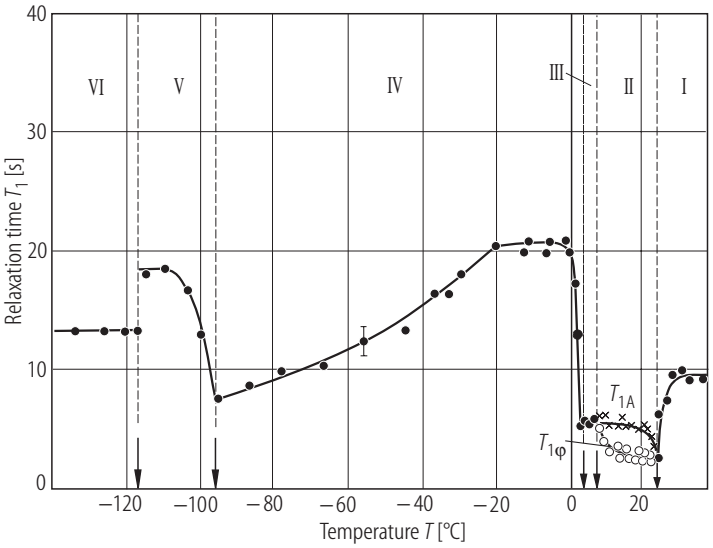

Fig. 39A-12-062. $[N(CH_3)_4]_2ZnCl_4$. T_1 vs. T [88Dol]. T_1: ^{14}N spin-lattice relaxation time. $T_{1\varphi}$, T_{1A}: the phason and the amplitudon contributions, respectively.

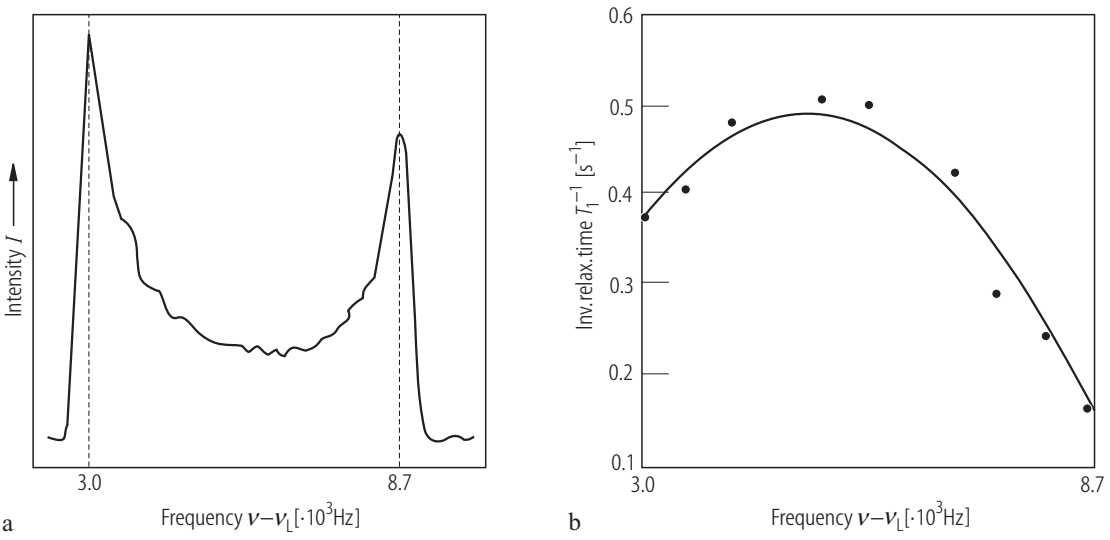

Fig. 39A-12-063. $[N(CH_3)_4]_2ZnCl_4$. (**a**) ^{14}N NMR spectra and (**b**) T_1^{-1} vs. $\nu - \nu_L$ [85Bli]. T_1: effective ^{14}N spin-lattice relaxation time. T = 14 °C. ν_L = 19.520 MHz. ***H*** ∥ ***b***.

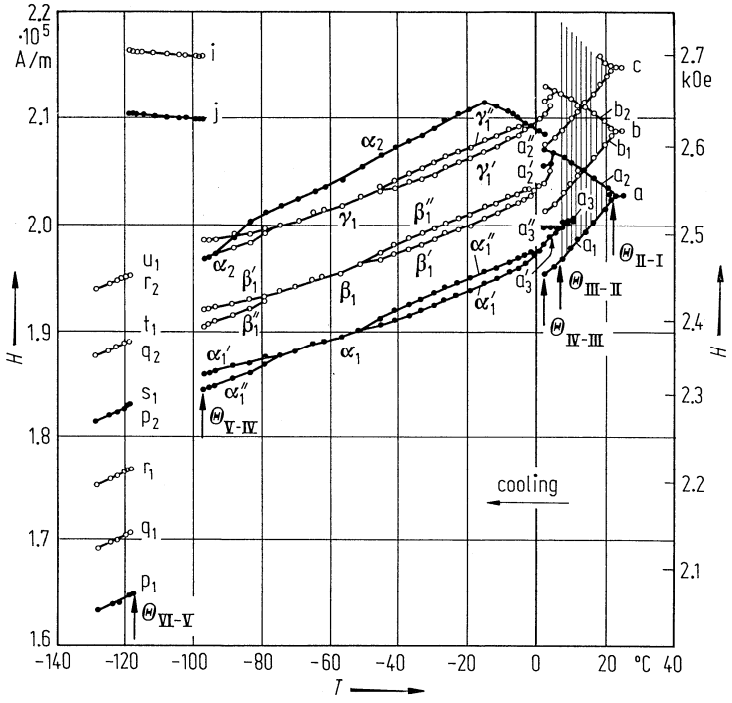

Fig. 39A-12-064. $[N(CH_3)_4]_2ZnCl_4$. *H* vs. *T* [83Mac]. *H*: resonance field for Mn^{2+} measured by X-band spectrometer. *H* is parallel to the principal axis *z* of the ***D***-tensor in phase I, see Table 39A-12-017. The full circles indicate the hyperfine lines assigned to the transitions between $|m_s = 5/2, m_I = 5/2>$ and $|m_s = 3/2, m_I = 5/2>$. Hatched region indicates continuous distribution of resonance fields. The symbols (a, b, c, ...) distinguish the different hyperfine lines. The same applies to (α, β, ...), (i, j, ...) and (p, q, ...).

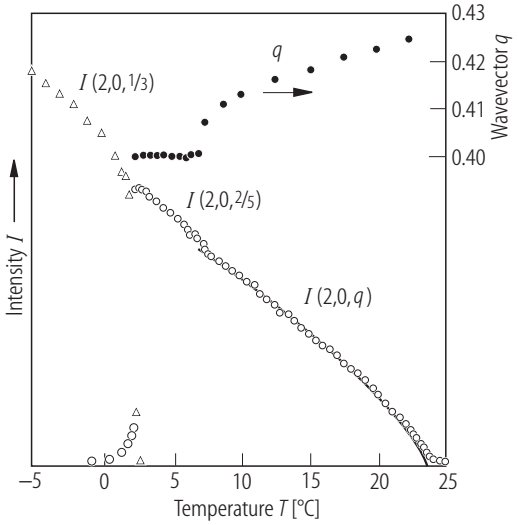

Fig. 39A-12-065. $[N(CH_3)_4]_2ZnCl_4$. I, q vs. T [80Mas2]. I: integrated intensity of X-ray diffraction. q: modulation wave vector in unit of c^*.

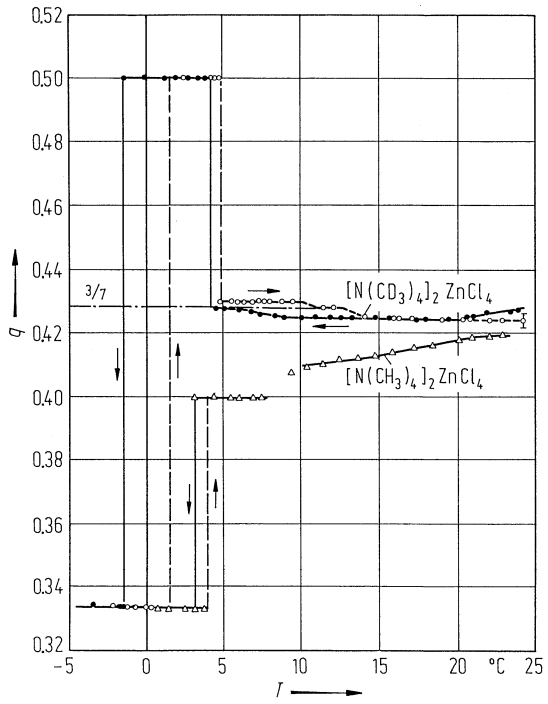

Fig. 39A-12-066. $[N(CH_3)_4]_2ZnCl_4$, $[N(CD_3)_4]_2ZnCl_4$. q vs. T [81Mar1]. q: modulation wave vector in unit of c^*.

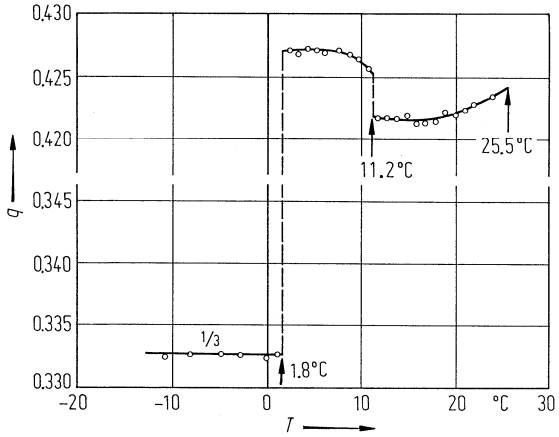

Fig. 39A-12-067. $[N(CD_3)_4]_2ZnCl_4$. q vs. T [83Iiz]. q: modulation wave vector in unit of c^*.

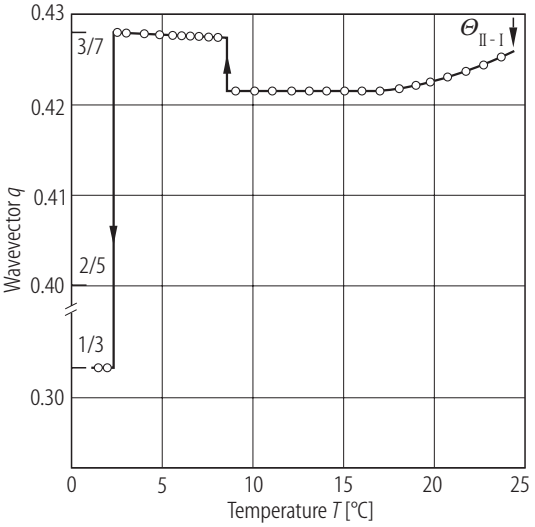

Fig. 39A-12-068. $[N(CD_3)_4]_2ZnCl_4$. q vs. T [88Dur]. q: modulation wave vector in unit of c^*.

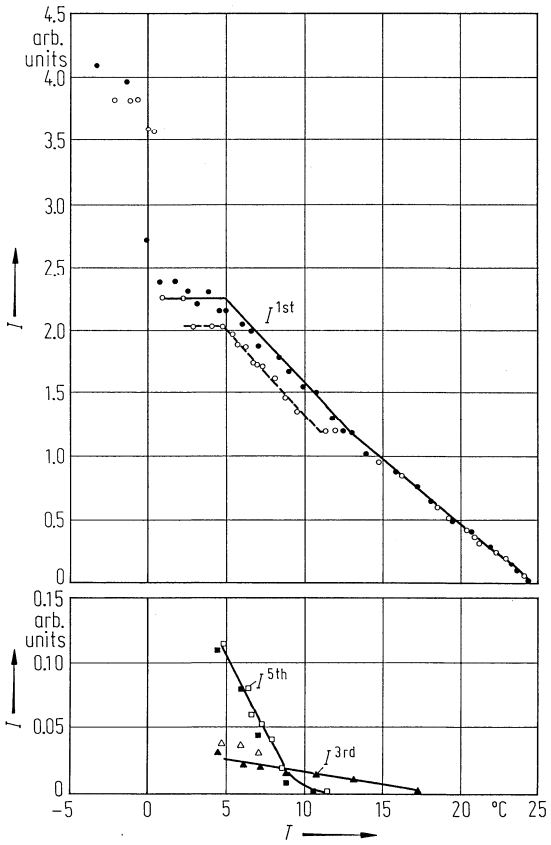

Fig. 39A-12-069. $[N(CD_3)_4]_2ZnCl_4$. I^{1st}, I^{3rd} I^{5th} vs. T [81Mar1]. I^{1st}: integrated intensity of the first order satellite of 200 reflection. I^{3rd}, I^{5th}: integrated intensity of (2, 0, 2 – 3q) and (2, 0, 2 – 5q) satellite reflection. Full and open symbols indicate cooling and heating process, respectively.

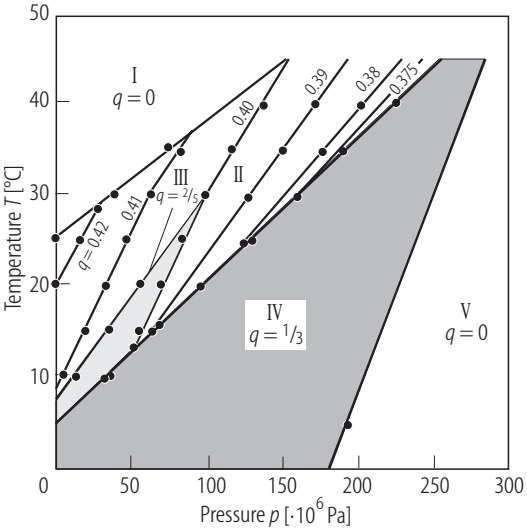

Fig. 39A-12-070. $[N(CH_3)_4]_2ZnCl_4$. Contour map of q on p–T plane [96Shi]. q: modulation wave vector in unit of c^*.

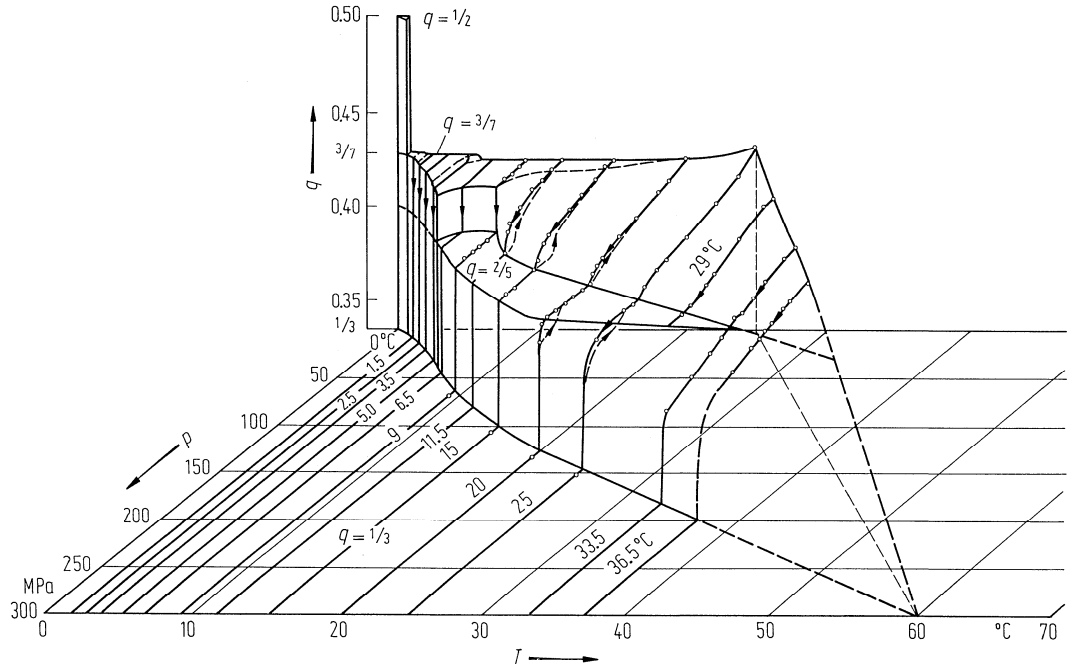

Fig. 39A-12-071. $[N(CD_3)_4]_2ZnCl_4$. q vs. p, T [84Mar2]. q: modulation wave vector in unit of c^*.

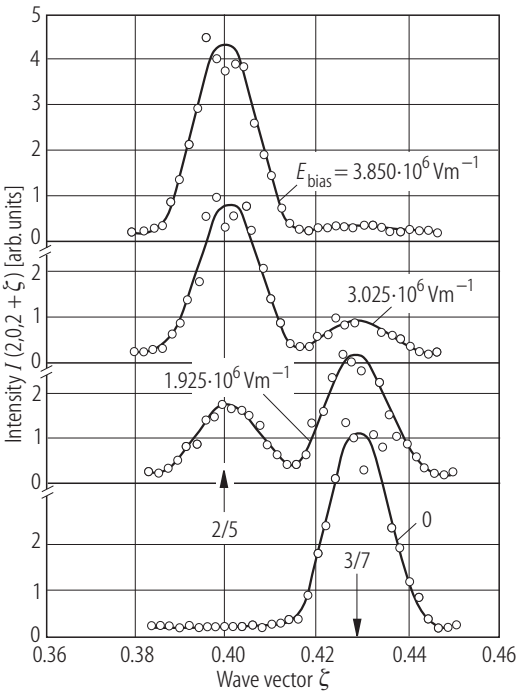

Fig. 39A-12-072. $[N(CD_3)_4]_2ZnCl_4$. I (2, 0, 2+ζ) vs. ζ at T = 3.4 °C [88Dur]. I(2, 0, 2+ζ): neutron diffraction intensity at (2, 0, 2+ζ). Parameter: E_{bias}.

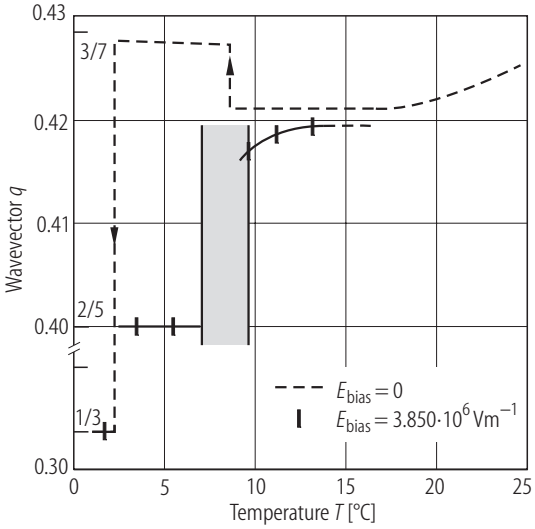

Fig. 39A-12-073. $[N(CD_3)_4]_2ZnCl_4$. q vs. T [88Dur]. q: modulation wave vector in unit of c^* for $E_{bias} = 3.850 \cdot 10^6$ V m^{-1} and 0.

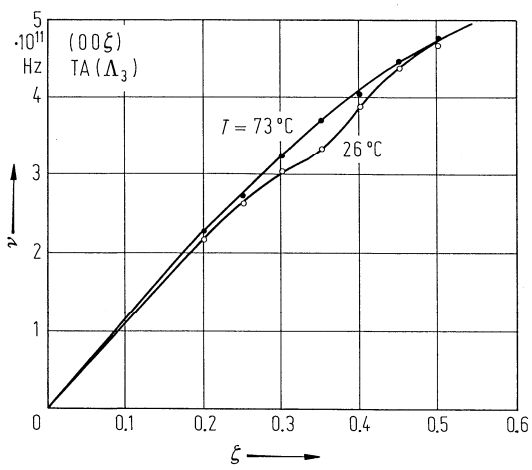

Fig. 39A-12-074. $[N(CD_3)_4]_2ZnCl_4$. ν vs. ζ [83Iiz]. ν: phonon frequency of the Λ_3 TA mode. ζ: reduced wave vector coordinate in unit of c^*.

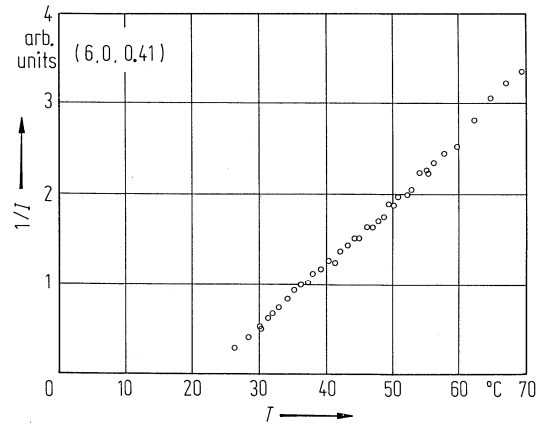

Fig. 39A-12-075. $[N(CD_3)_4]_2ZnCl_4$. $1/I$ vs. T [83Iiz]. I: quasielastic neutron scattering intensity at (6, 0, 0.41).

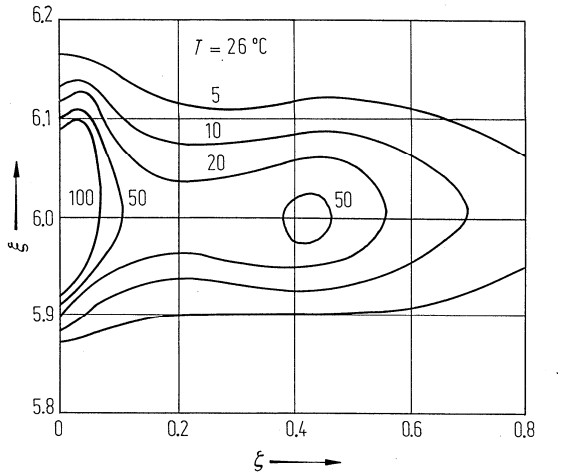

Fig. 39A-12-076. $[N(CD_3)_4]_2ZnCl_4$. Contour map of quasielastic neutron scattering on (ξ, 0, ζ) plane [83Iiz]. $T = 26$ °C.